Role of PEGylated lipid in lipid nanoparticle formulation for *in vitro* and *in vivo* delivery of mRNA vaccines

Li Zhang [a], Brandon Yi Loong Seow [a], Ki Hyun Bae [a], Yue Zhang [a], Kuo-Chieh Liao [b], Yue Wan [b], Yi Yan Yang [a, *]

[a] Bioprocessing Technology Institute (BTI), Agency for Science, Technology and Research (A*STAR), 20 Biopolis Way, #06-01 Centros, Singapore 138668, Republic of Singapore

[b] Genome Institute of Singapore (GIS), Agency for Science, Technology and Research (A*STAR), 60 Biopolis Street, #02-01 Genome, Singapore 138672, Republic of Singapore

Corresponding author at:

Bioprocessing Technology Institute (BTI), Agency for Science, Technology and Research (A*STAR), 20 Biopolis Way, #06-01 Centros, Singapore 138668, Republic of Singapore

* Email address: yyyang@bti.a-star.edu.sg (**Yi Yan Yang**)

Abstract

mRNA-loaded lipid nanoparticles (mRNA-LNPs) hold great potential for disease treatment and prevention. LNPs are normally made from four lipids including ionizable lipid, helper lipid, cholesterol, and PEGylated lipid (PEG-lipid). Although PEG-lipid has the lowest content, it plays a crucial role in the effective delivery of mRNA-LNPs. However, previous studies have yet to elucidate the key factors of PEG-lipid that influence the properties of LNPs. This study reported how PEG-lipid content, lipid tail length, and chemical linkage between PEG and lipid affected *in vitro* and *in vivo* properties of mRNA-LNPs. Forty-eight LNP formulations were prepared and characterized. The results revealed that a PEG-lipid molar content exceeding 3.0 % significantly reduced the encapsulation efficiency of mRNA in LNPs *via* manual mixing. An increased PEG-lipid content also significantly decreased mRNA translation efficiency. Although the chemical linkage had minimal impact, the lipid tail length of PEG-lipid significantly affected the properties of mRNA-LNPs, irrespective of whether the LNPs were prepared using manual or microfluidic mixing. mRNA-LNPs made from ALC-0159 with C14 lipid tails, which is used in Pfizer/BioNTech COVID-19 mRNA vaccines, or C16-Ceramide-PEG preferably accumulated in the liver, while mRNA-LNPs prepared from C8-Ceramide-PEG were largely found in the lymph nodes. In a mouse SARS-CoV-2 Delta variant spike protein-encoded mRNA vaccine model, mRNA-LNPs made from either C8-Ceramide-PEG or C16-Ceramide-PEG yielded comparable vaccination efficacy to mRNA-LNPs made from ALC-0159, while mRNA-LNPs formulated with DSPE-PEG with C18 lipid tails mediated lower vaccination efficacy. C16-Ceramide-PEG LNPs and DSPE-PEG LNPs induced higher anti-PEG antibody response than C8-Ceramide-PEG and ALC-0159 LNPs. All the LNPs tested did not cause significant toxicity in mice. These results offer valuable insights into the use of PEG-lipid in LNP formulations and suggest that C8-Ceramide-PEG holds potential for use in the formulation of mRNA vaccine-loaded LNPs.

Keywords: lipid nanoparticles; mRNA; lipid tail length; PEG-lipid content; immunogenicity

Highlights

- The lipid tail length of PEG-lipid played a crucial role in mRNA-LNPs delivery
- PEG-lipid molar ratio significantly affected mRNA encapsulation and translation
- Chemical linkage between PEG and lipid had minimal impact on mRNA translation
- LNPs' fabrication technique and mRNA size influenced the properties of mRNA-LNPs
- C8-Ceramide-PEG had similar immune responses to ALC-0159 mRNA-LNPs by s.c. injection

1. Introduction

Lipid nanoparticles (LNPs) have great potential for the delivery of therapeutic nucleic acids, including messenger RNA (mRNA), small interfering RNA (siRNA), and antisense oligonucleotides (ASO) [1, 2]. In 2018, the Food and Drug Administration (FDA) approved Onpattro® (Patisiran), the first siRNA-loaded LNPs, for the treatment of hereditary transthyretin mediated amyloidosis (hATTR) [3, 4]. With the global outbreak of coronavirus disease 2019 (COVID-19), tremendous effort has been made to develop mRNA vaccines using LNP technology. In 2020, the FDA and European Medicines Agency (EMA) granted emergency use authorization to Pfizer/BioNTech's (BNT162b2) and Moderna's (mRNA-1273) mRNA vaccines. These vaccines, which demonstrated high efficacy and safety, have been pivotal in the fight against COVID-19, and have spurred ongoing research in mRNA-loaded LNPs (mRNA-LNPs) platforms for gene therapy [5-7]. Beyond COVID-19, mRNA vaccines are being explored for other infectious diseases nowadays, including influenza, Zika virus, and cytomegalovirus, with several already advancing into clinical trials [8].

Compared to traditional vaccines such as live attenuated or replicating vaccines, mRNA vaccines offer several advantages including rapid development, robust immune response, lower cost, and adaptable mRNA size [9-11]. LNPs can be modified to target specific cells or organs, enhancing their effectiveness in treating various diseases [1, 12, 13]. Typically, LNPs consist of four lipid components: ionizable lipid, helper lipid, cholesterol, and PEGylated lipid (PEG-lipid) [14]. Ionizable lipid plays a key role by facilitating mRNA binding during formulation and mRNA release into the cytosol to exert therapeutic effects [15]. The widely used ionizable lipids include DLin-MC3-DMA, ALC-0315, SM-102, C12-200, and L319 [15, 16]. Helper lipid enhances the stability and promotes membrane fusion. Cholesterol modulates the rigidity and integrity, thereby enhancing the stability of LNPs. PEG-lipid prevents

aggregation and prolongs the blood circulation time of LNPs by reducing the uptake by the reticuloendothelial system (RES) [14, 17, 18].

In the structure of LNPs, the lipid moiety of PEG-lipid integrates into the lipid matrix, whereas the PEG moiety extends outward on the surface of LNPs [19]. While increasing the *in vivo* circulation time, the PEG-lipid in LNPs impedes cellular uptake and endosomal escape, creating a "PEG dilemma" [20]. Moreover, although at the lowest molar ratio among the four lipid components, PEG-lipid significantly influences the characteristics and performance of mRNA-LNPs through factors including PEG chain length, lipid tail length, molar ratio, and chemical linkage between PEG and lipid moieties [17, 21]. Lowering the molar ratio of PEG-lipid in LNPs enhanced the translation efficiency of mRNA-LNPs [22]. FDA-approved LNPs used DMG-PEG and ALC-0159 with C14 lipid tails for rapid detachment from LNPs' surface to enhance cellular uptake and mRNA release [23]. In comparison, DSPE-PEG with longer lipid tails (C18) has a longer blood half-life and was more commonly used in liposomes designed for the delivery of small-molecule anticancer drugs [24-26]. Additionally, PEG-lipid could also contribute to the side effects of LNPs. It has been reported that the lipid tails of PEG-lipid affected the production of anti-PEG antibodies, highlighting PEG-lipids' impact on the immunological response of LNPs [19].

However, the key factors of PEG-lipid that determine the performance of LNPs remain unclear. Most current studies have focused on specific aspects of how PEG-lipid influences nuclear acid delivery *via* LNPs, examining *in vitro* properties [27], *in vivo* protein expression [28], or anti-PEG antibody production [19]. A comprehensive evaluation of the role of PEG-lipid in mRNA-LNPs, encompassing both *in vitro* transfection and *in vivo* immunogenicity for vaccination, has yet to be reported. Meanwhile, studies on the effects of lipid carbon tail length of PEG-

lipid in mRNA delivery *via* LNPs have primarily compared C14 (DMG-PEG) and C18 (DSG-PEG) PEG-lipids with ester bond linkage, neglecting a broader range of lipid tail lengths and other chemical linkages between PEG and lipid moieties [28, 29]. This narrow focus constrains our understanding of the full potential of these variables. Addressing these research gaps could yield valuable insights into the broader impact of PEG-lipid on mRNA-LNPs, enhancing their utility for both vaccination and other therapeutic applications.

In this study, we aim to investigate the crucial factors of PEG-lipid that influence physiochemical properties and biological functions of mRNA-LNPs for vaccination, focusing on the evaluation of molar ratios, lipid tail length, and chemical linkages between PEG and lipid (**Figure 1**). Libraries of mRNA-LNPs were made from different PEG-lipids at varying molar ratios in combination with the ionizable lipid ALC-0315, the helper lipid DSPC, and cholesterol by using both manual- and microfluidic-mixing techniques [13]. ALC-0159 in Pfizer/BioNTech mRNA vaccines was evaluated alongside other PEG-lipids featuring diverse lipid tail lengths: C8, C14, C16, and C18 carbon tails. Furthermore, PEG-lipids with different chemical linkages between PEG and lipid moieties, including ester, carbamate, ceramide, and anionic phosphate linkers, were employed to assess their influences on mRNA-LNPs for vaccination. Specifically, Firefly luciferase (FLuc) mRNA-LNPs fabricated with different PEG-lipids at varying molar contents were characterized for particle size, polydispersity index, zeta potential, *in vitro* mRNA translation, and *in vivo* biodistribution after subcutaneous administration (s.c.). mRNA encoding the spike protein of the SARS-CoV-2 Delta variant was loaded into optimal LNP formulations, which were subsequently used to immunize mice with two doses *via* s.c. injection (**Figure 2**). Anti-spike IgG and neutralizing antibody responses were evaluated, and the effect of PEG-lipid on anti-PEG antibody response was investigated. In addition, the safety profiles of mRNA-LNPs were examined in mice.

2. Materials and methods

2.1 Reagents and materials

All the reagents and solvent used were of analytical grade unless stated. The ionizable lipid, 6-((2-hexyldecanoyl)oxy)-*N*-(6-((2-hexyldecanoyl)oxy)hexyl)-*N*-(4-hydroxybutyl)hexan-1-aminium (ALC-0315), methoxypolyethyleneglycoloxy(2000)-*N*,*N*-ditetradecylacetamide (ALC-0159), 1,2-dimyristoyl-*rac*-glycero-3-methoxypolyethylene glycol-2000 (DMG-PEG), 1,2-distearoyl-*sn*-glycero-3-methoxypolyethylene glycol-2000 (DMG-C-PEG), 1,2-distearoyl-*sn*-glycero-3-phosphocholine (DSPC), and cholesterol were purchased from MedChemExpress (Monmouth Junction, NJ, USA). *N*-octanoyl-sphingosine-1-succinyl[methoxy(polyethylene glycol)2000] (C8-Ceramide-PEG), 1,2-Dimyristoyl-*sn*-glycero-3-phosphoethanolamine-*N*-[methoxy(polyethylene glycol)-2000] ammonium (DMPE-PEG), *N*-palmitoyl-sphingosine-1-succinyl[methoxy(polyethylene glycol)2000] (C16-Ceramide-PEG), 1,2-distearoyl-*rac*-glycero-3-methylpolyoxyethylene (DSG-PEG), sodium phosphate, sodium borate, sodium citrate, sodium chloride, and 6-(*p*-toluidino)-2-naphthalenesulfonic acid sodium (TNS) were purchased from Sigma-Aldrich (St. Louis, MO, USA). 2-Distearoyl-*sn*-glycero-3-phosphoethanolamine-*N*-[carboxy(polyethylene glycol)-2000 (DSPE-PEG) was purchased from Biopharma PEG Scientific Inc. (Watertown, MA, USA). Tri-EDTA (TE) buffer, Quant-it™ RiboGreen RNA Assay Kit, Dulbecco′s Modified Eagle′s Medium (DMEM), fetal bovine serum (FBS), Penicillin/Streptomycin antibiotics, Pierce™ firefly luciferase glow assay kit, Hoechst 33342, and LysoTracker™ Green DND-26 were purchased from Thermo Fisher Scientific (Waltham, MA, USA). CleanCap® Firefly Luciferase mRNA (FLuc) was purchased from Trilink Biotechnologies (San Diego, CA, USA). Cy5-labeled firefly luciferase (Cy5) mRNA was purchased from APExBIO Technology LLC (Houston, TX, USA). cPass™ SARS-CoV-2 neutralization antibody detection kit and Delta variant SARS-CoV-2 spike protein were purchased from GenScript Biotech (Piscataway, NJ,

USA). SARS-CoV-2 Spike RBD Protein Sandwich Elisa Kit was purchased from GeneTex, Inc. (Irvine, CA, USA). VivoGlo™ Luciferin, In Vivo Grade was purchased from Promega (Madison, WI, USA). Goat anti-mouse IgG-Fc fragment antibody-HRP conjugate (Catalog No.: A90-131P) and goat anti-mouse IgM antibody-HRP conjugate (Catalog No.: A90-101P) were purchased from Bethyl Laboratories (Montgomery, TX, USA). KPL SureBlue Reserve™ 1-Component TMB Microwell Peroxidase Substrate and TMB stop solution were purchased from SeraCare Life Sciences Inc. (Milford, MA, USA).

2.2 mRNA synthesis

For the synthesis of mRNA encoded for the spike protein of the SARS-CoV-2 Delta variant, 0.5-1 mg linearized plasmids were used as template for RNA synthesis using HiScribe T7 High Yield RNA synthesis kit (NEB) with following modifications: CleanCap AG (3' OMe) (Trilink-7413) was added to a final concentration of 4 mM and N1-Methylpseudouridine-5'-Triphosphate (m1y) (Trilink N1081) was fully substituted for UTP. Reactions were incubated at 37 °C for 2 h and *in vitro* transcription (IVT) templates were subsequently degraded with 2 mL DNase I (Thermo Fisher Scientific, MA, USA) per IVT reaction for 30 min at 37°C. The remaining RNA is then column purified. After column clean up, these RNA samples were further purified using POROSTM Oligo (dT)25 affinity resin (Thermo Fisher Scientific, MA, USA) according to the manufacturer's instructions.

2.3 Preparation of mRNA-LNPs

The mRNA-LNPs were formulated by rapid mixing of an aqueous phase and an organic phase. The aqueous contained diluted mRNA with 1 mM sodium acetate buffer at pH 5.2. The organic phase comprised lipids dissolved in ethanol solution. The lipid mixture comprised ALC-0315: DSPC: cholesterol: respective PEG-lipid at a molar ratio of 46.3:9.4:(44.3-X) :X, where X

ranged from 0.5 to 10. The N/P ratio was fixed at 6. The volume ratio of the aqueous phase to the organic phase was set at 3.

For manual mixing, FLuc mRNA was used in the aqueous phase. The two phases were rapidly mixed by a pipette and then placed at room temperature for 20 min to allow for self-assembly. The LNPs were subjected to buffer dilution to solidify the LNPs by decreasing ethanol concentration [30]. For microfluidic mixing, FLuc mRNA, Cy5 mRNA, and mRNA encoded for the spike protein of the SARS-CoV-2 Delta variant were dispersed in the aqueous phase, respectively. The aqueous phase and organic phase were mixed at a total flow rate of 12 mL/min through a NanoAssemblr Benchtop (Precision Nanosystems, Vancouver, Canada). The flow rate ratio of the aqueous phase to the organic phase was 3. The resulting LNPs were diluted 40 times with phosphate-buffered saline (PBS), concentrated by ultracentrifugation tubes with a molecular weight cut-off of 30,000 Da at 1500 g and 4 °C to less than 1 mL, and stored at 4 ℃ for future use.

2.4 Characterization of mRNA-LNPs

Dynamic light scattering (DLS) was utilized to measure the Z-average size, polydispersity index (PDI), and zeta potential of mRNA-LNPs using Malvern Zetaszier Ultra (Malvern, UK). 10 μL of mRNA-LNPs' suspension was diluted to 1 mL with PBS and measured in triplicate at 25 °C. The encapsulation efficiency (EE) of mRNA in LNPs was quantified with Quant-it™ RiboGreen RNA Assay Kit. The calibration curve was prepared with serial dilution of mRNA standards. 10 μL of mRNA standard or diluted mRNA-LNPs were added to a 96-well black plate. 90 μL of 200-fold diluted Ribogreen reagent in TE buffer with or without 0.5 % Triton X-100 was added and incubated for 20 min at 37 °C. The fluorescence intensity was read by a

microplate reader (Tecan, Switzerland) at the excitation wavelength of 485 nm and emission wavelength of 535 nm. The EE of mRNA in LNPs was calculated by the following equation:

$$EE\% = \frac{mRNA_{with\ Triton} - mRNA_{without\ Triton}}{mRNA_{with\ Triton}} \times 100\%$$

where $mRNA_{with\ Triton}$ is the mRNA concentration measured with Triton X-100, and $mRNA_{with\ Triton}$ is the mRNA concentration measured without TritonX-100.

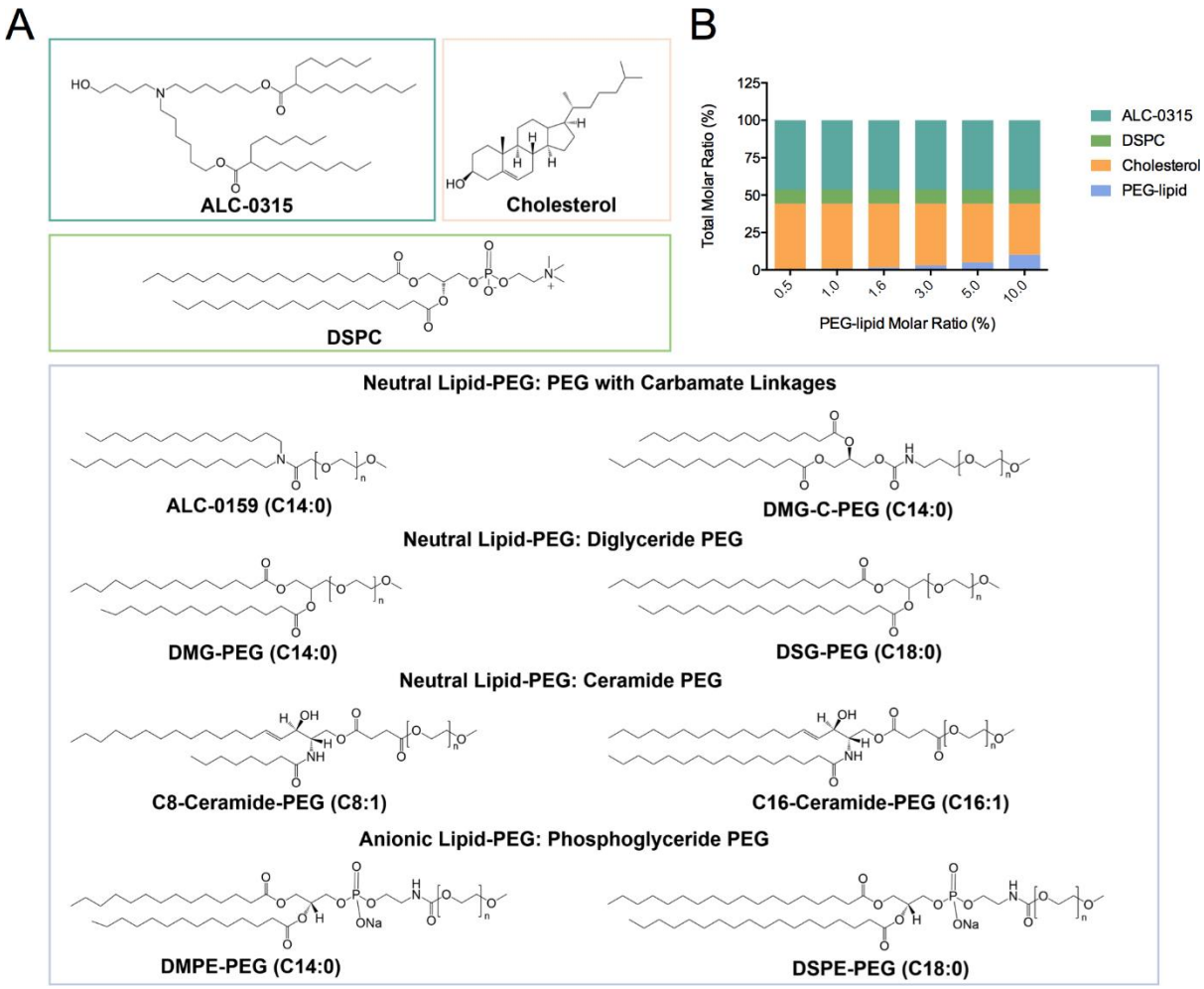

Figure 1. Investigation of influences of PEG-lipid on the *in vitro* and *in vivo* performance of mRNA-LNPs vaccines. (A) A diverse library of ionizable lipid, DSPC, cholesterol, and PEG-lipid used for the preparation of mRNA-LNPs. (B) Molar compositions of LNPs made from the four lipid components. (C) Schematic of preparation of mRNA-LNPs formulated *via* manual- or microfluidic-mixing. (D) Optimal LNPs selected from *in vitro* screening for *in vivo* evaluation *via* s.c injection.

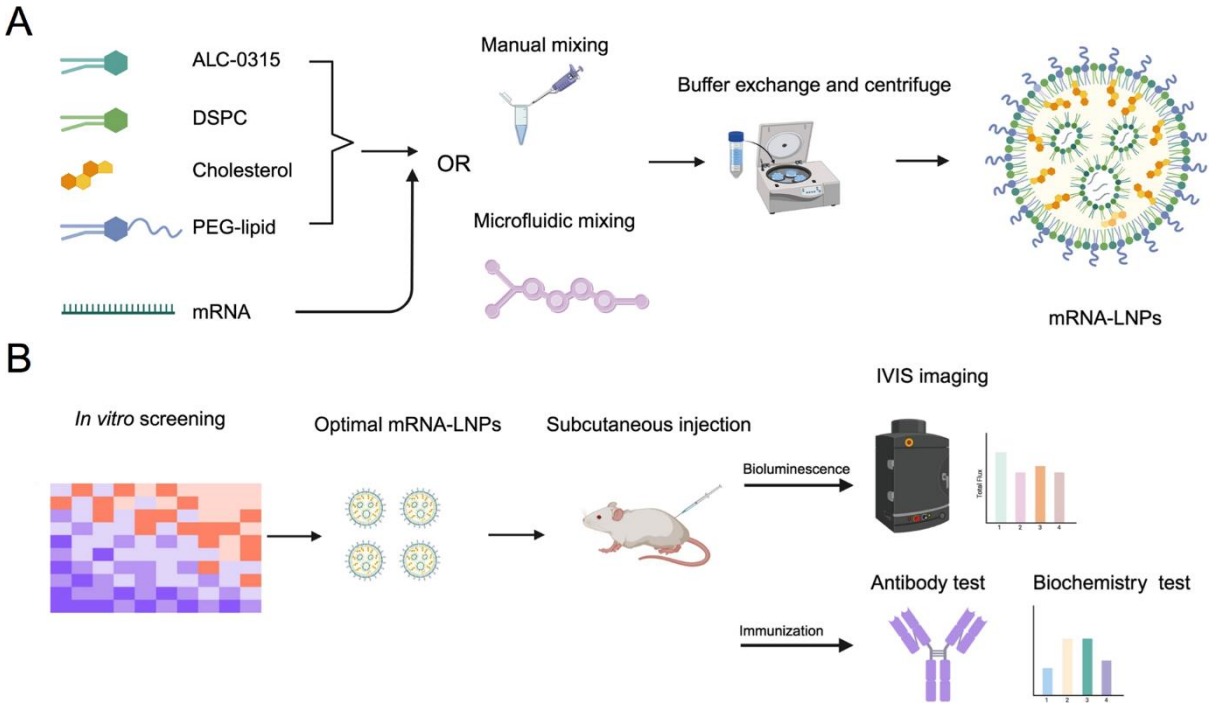

Figure 2. Schematic of *in vitro* and *in vivo* evaluation of mRNA-LNPs. (A) Preparation of mRNA-LNPs formulated *via* manual- or microfluidic-mixing. (B) Optimal LNPs selected from *in vitro* screening for *in vivo* evaluation *via* s.c injection.

2.5 Hemolysis assay

The hemolysis assay was conducted with the freshly collected mouse red blood cells (RBCs) [31]. The RBCs were washed with saline three times and diluted to 2.0×10^8 cells/mL. The LNPs were diluted with PBS under different pH to the total lipids' concentration of 60 μM. 250 μL of diluted LNPs were mixed with 250 μL of RBCs and incubated at 37 ºC for 30 min. The mixture was centrifuged at 1000 rcf and 4 ºC for 5 min. Then 100 μL of supernatant was transferred to a 96-well plate and the absorbance (ABS) was read at 576 nm by a microplate reader (Tecan, Switzerland). Saline was used as the negative control and 0.5% Triton-X100 was used as the positive control. The hemolysis rate was calculated by the following equation:

$$Hemolysis\% = \frac{\mathrm{ABS_{treated\ sample}} - \mathrm{ABS_{negative\ control}}}{\mathrm{ABS_{positve\ control}} - \mathrm{ABS_{negative\ control}}} \times 100\%$$

where $\mathrm{ABS}_{treated\ sample}$ is the absorbance of the treated sample group, $\mathrm{ABS}_{negative\ control}$ is the absorbance of the negative control group, and $\mathrm{ABS}_{positive\ control}$ is the absorbance of the positive control group.

2.6 Apparent pKa measurement

The apparent acid dissociation constant (pKa) of LNPs was determined with 300 µM TNS reagent dissolved in dimethylsulfoxide (DMSO). A buffer solution of 10 mM sodium phosphate, 10 mM sodium borate, 10 mM of sodium citrate, and 150 mM sodium chloride was prepared, and pH was adjusted from pH 3 to 10 in increments of 0.5 pH with 0.1 M sodium hydroxide or hydrochloric acid. In a 96-well black plate, 90 µL of each buffer solution was mixed with 3.26 µL of mRNA-LNPs and 2 µL of TNS solution. The fluorescence was measured immediately with an excitation wavelength of 321 nm and an emission wavelength of 445 nm. The actual pH of each well was verified by a micro pH electrode (Mettler Toledo, Melbourne, Australia). The apparent pKa of LNPs was calculated as the pH value at 50 % of the fluorescence intensity on fluorescence intensity versus pH curve.

2.7 Stability of mRNA-LNPs in the presence of serum

The mRNA-LNPs were diluted with PBS to the final mRNA concentration of 70 ng/µL. Then the mRNA-LNPs' suspension was mixed with an equal volume of 20 % FBS to reach 10 % FBS. The mixture was incubated at 37 °C under gentle shaking. At time points of 0.5, 1, 2, 4, 24, and 48 h, 20 µL of the mixture was diluted to 1 mL with PBS. The size, PDI, and zeta potential of mRNA-LNPs were measured by DLS, as described in Section 2.4.

2.8 Cell culture

Human hepatoblastoma carcinoma (HepG2) and adenocarcinoma alveolar basal epithelial (A549) cell lines (ATCC, USA) were maintained in a DMEM medium supplemented with 10 % FBS and 1 % penicillin/streptomycin. The cells were cultured in an incubator maintained at 37 °C in a humid atmosphere containing 5 % CO_2.

2.9 Cell viability

For FLuc mRNA-loaded LNPs, 10,000 cells per well (100 µL) were seeded onto a 96-well black plate with a transparent bottom and incubated overnight. The medium was replaced with cell culture medium containing LNPs at a dose of 100 ng mRNA per well for 48 h. For the LNPs loaded with mRNA encoding SARS-CoV-2 Delta variant spike protein, 100,000 cells per well (1 mL) were seeded onto a 12-well plate and treated similarly.

After mRNA-LNPs treatment, the fresh medium containing 10 % (*V/V*) Alamar Blue reagent was replaced and incubated for another 2 hours. The fluorescence intensity was measured with the microplate reader (Tecan, Switzerland) at an excitation wavelength of 570 nm and an emission wavelength of 600 nm. The cell viability of each treated group was compared to the untreated group.

2.10 In vitro mRNA translation assay

For FLuc mRNA-loaded LNPs, the cells were seeded onto a 96-well plate (a white plate with a transparent bottom). After 48 h treatment as mentioned above, the cell culture medium was removed, and the luminescence intensity was measured with Pierce™ firefly luciferase glow assay kit. 50 µL of cell lysis buffer and 50 µL of D-luciferin (60 mg/mL) in the firefly glow assay buffer were added. After 10 min incubation at 37 °C, the luminescence intensity was measured *via* the microplate reader (Tecan, Switzerland) with an exposure time of 1000 ms. The protein amount was quantified *via* Pierce™ BCA assay protein kit. The normalized translation efficiency of mRNA was expressed as the relative light unit (RLU) per mg of protein.

For the LNPs loaded with mRNA-encoded spike protein of SARS-CoV-2 Delta variant, the cell culture medium was collected and centrifuged at 1,500 rpm for 10 min at 4 °C after 48 h treatment. The spike protein concentration in the cell culture supernatant was tested with GeneTex SARS-CoV-2 Spike RBD Protein Sandwich Elisa Kit.

2.11 Confocal live cell imaging

To visualize the cellular uptake and the localization of mRNA-loaded LNPs, the 10,000 cells were seeded onto an 8-well Nunc™ Lab-Tek™ Chamber Slide™ system. After attachment overnight, the cells were dosed with 1 mL of cell culture medium containing Cy5 mRNA-loaded LNPs at a dose of 2 µg mRNA per well and incubated for 6 h. The cells were washed with PBS two times and incubated with 500 nM LysoTracker™ Green DND-26 staining solution for 1 h to stain the lysosomes. After washing with PBS three times, the cells were further incubated with 10 µg/mL Hoechst 33342 for 10 min to stain the nuclei. The images were obtained by an FV3000 confocal laser scanning microscopy (Olympus, Tokyo, Japan). The fluorescent images were analyzed by Image J.

2.12 In vivo bioluminescence study

All the animal studies were conducted under the Institutional Animal Care and Use Committee (IACUC) of the Singapore Biological Center with the protocol number 221681. Female BALB/c mice aged 5 to 6 weeks were obtained from *InVivos* (Singapore). The mice were housed in a pathogen-free animal facility at standard conditions such as humidity of 60-70 %, temperature of 22 ± 1 °C, 12 h light/dark cycle, and free access to food and water. The mice were injected with FLuc mRNA-LNPs subcutaneously in the hind leg at a dose of 1 µg of mRNA per mouse. At different time points, 200 µL of VivoGlo D-luciferin (15 mg/mL) was injected intraperitoneally. Imaging was performed with an IVIS Spectrum imaging system

(PerkinElmer, Waltham, MA, USA) after 10 min. At the end of *in vivo* imaging, the tissues including the heart, liver, spleen, lung, kidney, inguinal lymph node, and skin were collected for *ex vivo* imaging immediately. The total luminescence of the region of interest was quantified with the Living Imaging software (PerkinElmer, Waltham, MA, USA).

2.13 In vivo immunization study

The female BALB/c mice were subcutaneously immunized with LNPs loaded with mRNA encoding for the spike protein of SARS-CoV-2 Delta variant in the hind leg at the dose of 500 ng mRNA per mouse with a prime-boost strategy. The two doses were injected at an interval of 3 weeks. The blood was collected every week by cheek bleeding to obtain serum by centrifugation. The serum was stored at - 80 °C for different antibody tests. The body weight was recorded every week as well. The whole experiment ended at week 11 by euthanasia with CO_2. The serum was collected for biochemistry analysis including albumin, alkaline phosphatase (ALP), alanine aminotransferase (ALT), creatine kinase-MB (CK-MB), creatinine, total proteins, and urea.

2.14 ACE2-RBD binding inhibition ELISA and anti-spike IgG antibody response

The serum was collected to evaluate the antibody response triggered by mRNA-LNPs. The level of total neutralizing antibodies to block the interaction between the SARS-CoV-2 RBD domain and human angiotensin-covering enzyme 2 (ACE2) receptors on host cells was tested by the SARS-CoV-2 Surrogate Virus Neutralization Test Kit. The serum was diluted 10 times. The assay was performed according to the instructions of the manufacturer. The percentage of inhibition was considered positive when higher than 30 %.

To assess the anti-spike IgG titer, the spike protein of the SARS-CoV-2 Delta variant was diluted with carbonate buffer (pH 9.6) to 250 ng/mL. 100 µL of diluted protein solution was coated on MaxiSorp 96-well plates (Thermo Fisher Scientific, MA, USA) overnight at 4 °C, followed by washing 2 times with 1 % (*W/W*) bovine serum albumin (BSA) in PBS twice. The plates were blocked with 4 % BSA in PBS for 2 h at 37 °C. 100 µL of diluted serum samples were added at 1:5 serial dilution factor in 1 % BSA at a starting dilution factor of 200 times for 2 h at 25 °C. After washing with 1% BSA in PBS 3 times, goat anti-mouse IgG-Fc fragment antibody-HRP conjugate was added at 1:8000 dilutions for 1 h. Then the plates were washed with PBS 5 times. 100 µL of TMB substrate was added to each well and incubated for 15 min in the dark. The color reaction was stopped by adding TMB stop solution. Finally, the absorbance of the plates was read at 450 nm by the microplate reader (Tecan, Switzerland). The endpoint titer was calculated as the dilution gives a signal at least 3 times higher than the mean signal background.

2.15 Anti-PEG antibody response

For the detection of anti-PEG antibodies, 50 µL of NH_2-PEG_{3K}-NH_2 (200 µg/mL) was coated onto the MaxiSorp plates overnight at 4 °C [32]. The serum samples were added at 1:2 serial dilution factor in 1 % BSA at a starting dilution factor of 10 times for 2 h at 25 °C. The goat anti-mouse IgM antibody-HRP conjugate and goat anti-mouse IgG-Fc fragment antibody-HRP conjugate were added, respectively, at 1:3000 dilutions for the detection of anti-PEG IgM and IgG antibodies.

2.16 Statistics

All the data were reported as mean ± standard deviation (SD) otherwise indicated. One-way or Two-way analysis of variance (ANOVA) with the Tukey test was used for multiple group

comparison. Data analysis was performed with GraphPad Prism 10 software (GraphPad Software, San Diego, CA, USA). The significant difference was defined when $p < 0.05$ (* $p < 0.05$, ** $p < 0.01$, and *** $p < 0.001$). N.S. represented no significant difference between or among the tested groups.

3. Results

3.1 Physicochemical properties of FLuc mRNA-LNPs prepared via manual mixing

The lipid components (ALC-0315, DSPC, cholesterol, and ALC-0159) of Pfizer/BioNTech (BNT162b2) were used as the "standard" formulation. **Figure 3** shows the physicochemical characterization of mRNA-LNPs with different PEG-lipids *via* manual mixing. The average size of the "standard" formulation at 1.6 % ALC-0159 was 183.3 ± 1.5 nm. Increasing the molar content of PEG-lipids from 0.5 to 10.0 % resulted in a decreasing trend in the average size of LNPs, indicating more compact LNPs formed at high molar contents of PEG-lipids (**Figure 3A**). However, DSPE-PEG, which possessed the longest lipid tails among the tested PEG-lipids and a negative charge, showed a distinct behavior compared to other PEG-lipids in the formulation of LNPs. The average size increased from 165.1± 1.5 at 0.5 % DSPE-PEG to 277.7 ± 31.6 and 446.3 ± 44.2 nm at 5 % and 10% DSPE-PEG, respectively, indicating changes in packing of LNPs. A similar trend was observed in PDI for LNPs formed from most PEG-lipids, except those containing negatively charged PEG-lipids (DMPE-PEG and DSPE-PEG) (**Figure 3B**). LNPs formed with 5 % and 10 % DMPE-PEG or DSPE-PEG exhibited significantly higher PDI than those prepared with lower molar contents of these PEG-lipids likely due to charge repulsion hindering the efficient packing of the LNPs. The surface of all mRNA-LNPs in the LNP library exhibited zeta potential values within a range of ±10 mV (**Figure 3C**). The encapsulation efficiency of mRNA in most LNP formulations was around 80% at 0.5-1.6% of PEG-lipids, but it dramatically decreased when 3-10% of PEG-lipids were

used (**Figure 3D**). Therefore, these results indicated that at 0.5-3.0% of PEG-lipids, neither the chemical linker between PEG and lipid tails nor the lipid tail length significantly affected the average size and PDI of mRNA-LNPs, while at 5% and 10% of PEG-lipids, the average size and PDI increased for mRNA-LNPs formed from the PEG-lipids with the phosphate linker. In addition, the encapsulation efficiency of mRNA in LNPs was primarily influenced by the molar content of PEG-lipids.

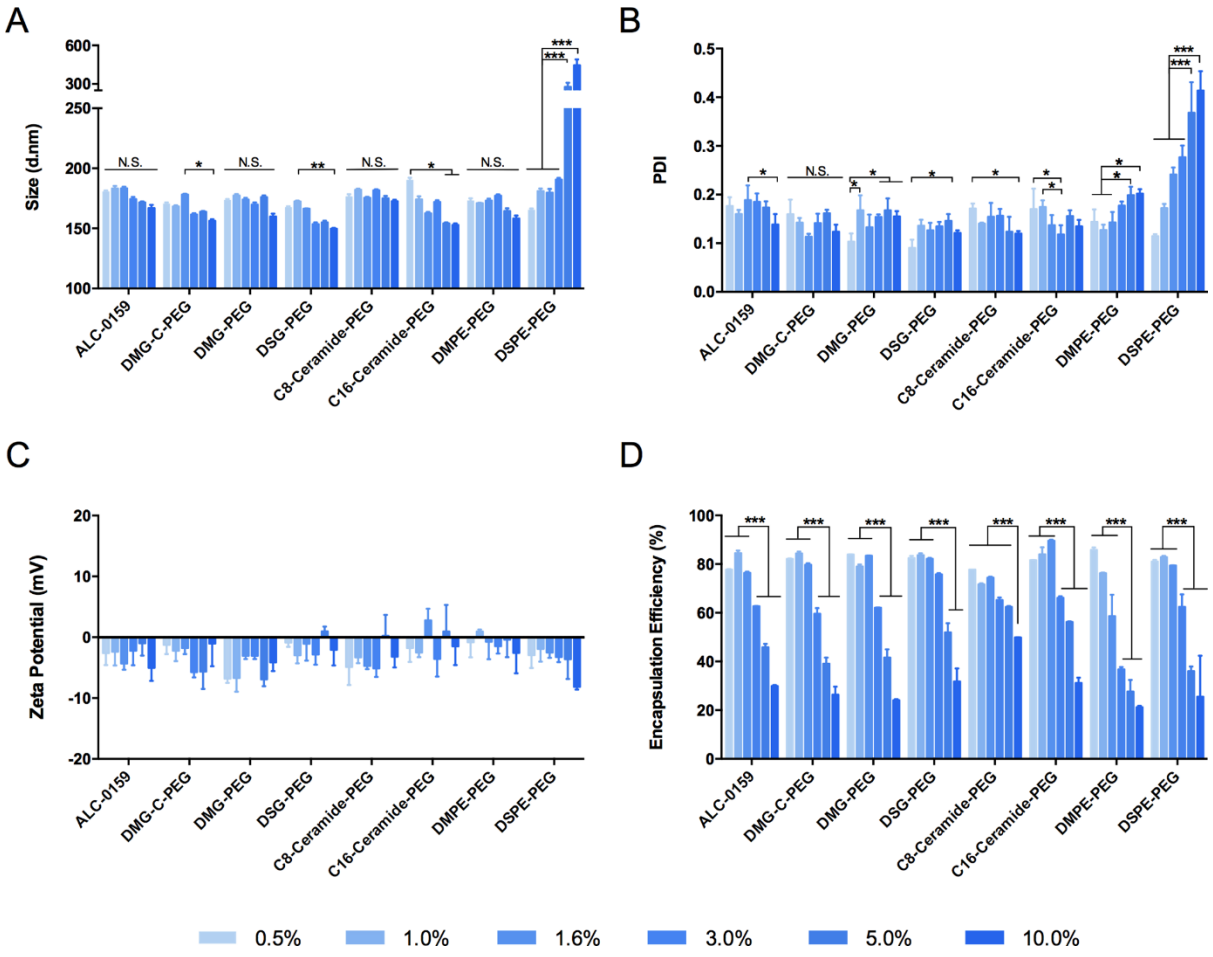

Figure 3. Physicochemical properties of FLuc mRNA-LNPs prepared with different PEG-lipids at varying molar contents *via* manual mixing, including size (A), PDI (B), zeta potential (C), and encapsulation efficiency (D). (*n* = 2-3 per group).

3.2 In vitro cytocompatibility and translation of FLuc mRNA-LNPs prepared via manual mixing

Figure 4 shows that HepG2 and A549 cells had viability higher than 90 % after incubating with the mRNA-LNPs across the library, indicating their high cytocompatibility. mRNA

translation efficiency is cell-type dependent. It also showed a notable correlation to the molar content of PEG-lipid in mRNA-LNPs. Compared to the "standard" mRNA-LNPs prepared with 1.6 % ALC-0159, reducing ALC-0159 to 0.5 % increased the luminescence intensity to 2.54-fold, while increasing ALC-0159 to 10.0 % decreased the luminescence intensity to 0.22-fold in HepG2 cells (**Figure 4**). The rest PEG-lipids exhibited a similar trend; the higher PEG molar contents resulted in lower luminescence intensity. Although some variations were observed in A549 cells, the general trend was in agreement with HepG2 cells (**Figure 4**).

When evaluating the effect of lipid tail length in the normalized luminescence intensity of mRNA-LNPs, the PEG-lipids with shorter lipid tail lengths yielded significantly higher luminescence intensity in HepG2 cells: at 1.6 %, C8-Ceramide-PEG *vs.* C16-Ceramide-PEG, 6.21-fold; DMG-PEG *vs.* DSG-PEG, 20.57-fold; DMPE-PEG *vs.* DSPE-PEG, 49.25-fold (**Figure S1A**). The luminescence intensity in A549 cells further confirmed the trend (**Figures 4 & S1B**).

Unlike the lipid tail length and molar content of PEG-lipid, the chemical linker between PEG and lipid tails showed limited influences on the translation efficiency of mRNA-LNPs. As shown in **Figure S2**, the normalized luminescence intensity of mRNA-LNPs formed from 1.6 % DMG-C-PEG with the carbamate linker was 1.70-fold and 1.25-fold to that of mRNA-LNPs formed from 1.6 % DMG-PEG in HepG2 and A549 cells, respectively. The limited changes in normalized luminescence intensity were also observed for mRNA-LNPs formed from 1.6 % DMG-PEG and DMPE-PEG with the phosphate linker. The mRNA-LNPs formulated with 1. 6 % DMG-PEG exhibited 1.35-fold and 1.14-fold higher translation efficiency to those mRNA-LNPs formed from 1.6 % DMPE-PEG in HepG2 and A549 cells, respectively. Our results underlined the lipid tail length and molar content of PEG-lipid had a more significant influence

on mRNA translation efficiency than the chemical linker between PEG and lipid tails, especially the lipid tail length of PEG-lipid.

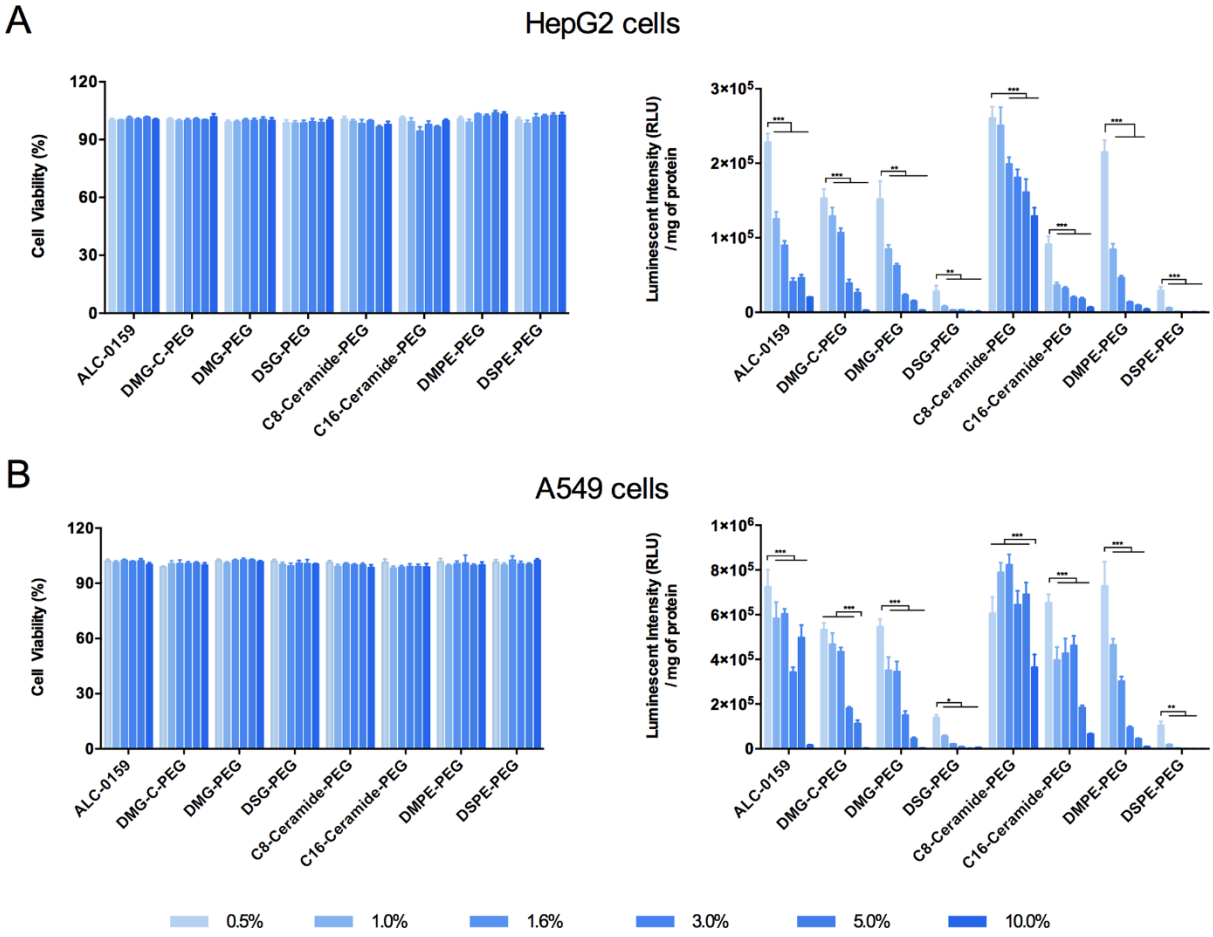

Figure 4. Cytocompatibility and normalized translation efficiency of FLuc mRNA-LNPs prepared with different PEG-lipids at varying molar contents *via* manual mixing in HepG2 (A) and A549 (B) cells. (n = 4-5 per group).

3.3 Physicochemical properties and in vitro translation efficiency of mRNA-LNPs prepared via microfluidic mixing

FLuc mRNA-LNPs were further prepared *via* microfluidic mixing as it can produce LNPs with well-controlled particle size and reproducibility for animal study [33]. A 1.6 % molar content of PEG-lipid was utilized as it gave high mRNA encapsulation efficiency (**Figure 3**) and translation efficiency (**Figure 4**). In addition, it is consistent with Pfizer-BioNTech's COVID-19 mRNA vaccine formulation [24]. The size of mRNA-LNPs formulated by microfluidic mixing was much smaller than those by manual mixing, all below 75 nm except for DSPE-

PEG (92.8 nm) (**Figure 5A**). All LNPs were highly monodisperse with PDI values below 0.2 and C8-Ceramide-PEG with the shortest lipid tails showed the largest PDI. Similar to mRNA-LNPs prepared *via* manual mixing, the chemical linker (DMG-PEG *vs.* DMG-C-PEG, DMG-PEG *vs.* DMPE-PEG) had a minimal effect on particle size and PDI (**Figure 5B**). However, the lipid tail length significantly influenced particle size and PDI. Comparing C8-Ceramide-PEG with C16-Ceramide-PEG having a longer lipid tail, C16-Ceramide-PEG yielded LNPs with significantly lower PDI. On the other hand, DMPE-PEG with shorter lipid tails formed LNPs with smaller size and lower PDI than DSPE-PEG LNPs. The zeta potential values of all mRNA-LNPs were within a range of ±10 mV (**Figure 5C**), suitable for *in vivo* application. The encapsulation efficiency of most LNP formulations prepared by microfluidic mixing was around 80 % (**Figure 5D**).

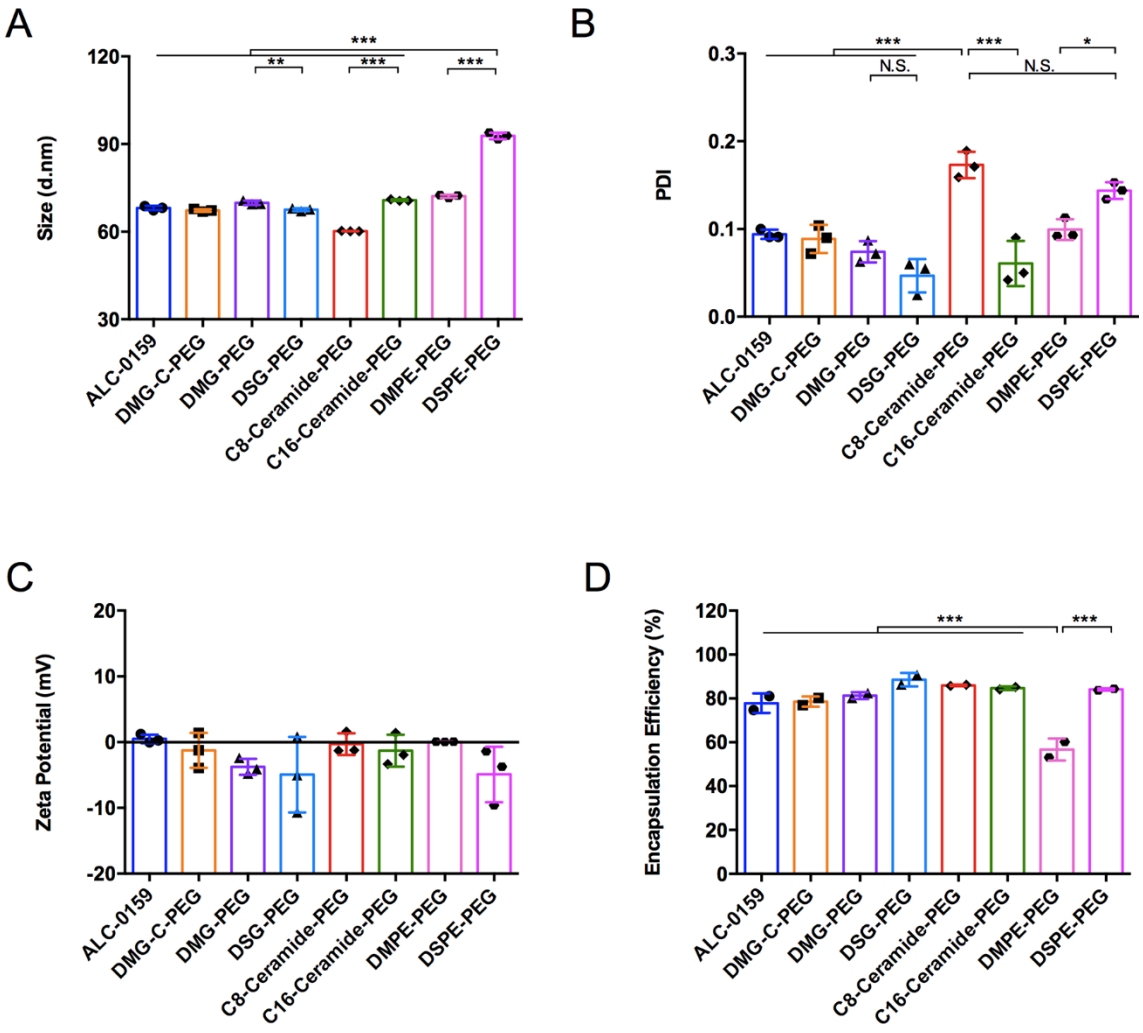

Figure 5. Physicochemical properties of FLuc mRNA-LNPs prepared with different PEG-lipids at 1.6 % molar content *via* microfluidic mixing, including size (A), PDI (B), zeta potential (C), and encapsulation efficiency (D). (n = 2-3 per group).

Similar to the mRNA-LNPs made *via* manual mixing, the treatment with the mRNA-LNPs prepared *via* microfluidic mixing led to comparable viability of both HepG2 and A549 cells, more than 70 % (**Figure 6**). In contrast to manual mixing, the mRNA translation efficiency increased to 9.36-fold in HepG2 cells and 4.92-fold in A549 cells when delivered by LNPs formed with 1.6 % of ALC-0159 *via* microfluidic mixing (**Figure 6**). In general, mRNA-LNPs made from PEG-lipids with different chemical linkers between PEG and lipid tails (DMG-PEG *vs.* DMG-C-PEG, DSG-PEG *vs.* DSPE-PEG) *via* microfluidic mixing exhibited limited mRNA translation efficiency variations in both cell lines as manual mixing. However, mRNA-LNPs

made from PEG-lipids with C18 lipid tails mediated significantly lower mRNA translation efficiency than those made from PEG-lipids with C14 lipid tails (DMG-PEG *vs.* DSG-PEG, DMPE-PEG *vs.* DSPE-PEG) in both cell lines. Interestingly, unlike manual mixing, mRNA-LNPs made from C8-Ceramide-PEG with a shorter lipid tail *via* microfluidic mixing exhibited a lower luciferase translation efficiency than those prepared with C16-Ceramide-PEG. These findings suggested the preparation method of mRNA-LNPs could influence the performance of LNPs, and most PEG-lipids led to comparable mRNA translation efficiency as ALC-0159 except for PEG-lipids with C18 lipid tails and C8-Ceramide-PEG *via* microfluidic mixing.

From the *in vitro* results, lipid tail length was a crucial factor influencing the performance of mRNA-LNPs. Therefore, four PEG-lipids with different lipid tail lengths (C8 to C18) were selected to prepare LNPs for further studies. C8-Ceramide-PEG and C16-Ceramide-PEG were selected as they have different lipid tail lengths while the same chemical linker between PEG and lipid tails. DSPE-PEG was selected as it led to the lowest translation efficiency in both cell lines tested, and it would be interesting to further study the corresponding *in vitro* and *in vivo* behavior. ALC-0159 was chosen as a positive control.

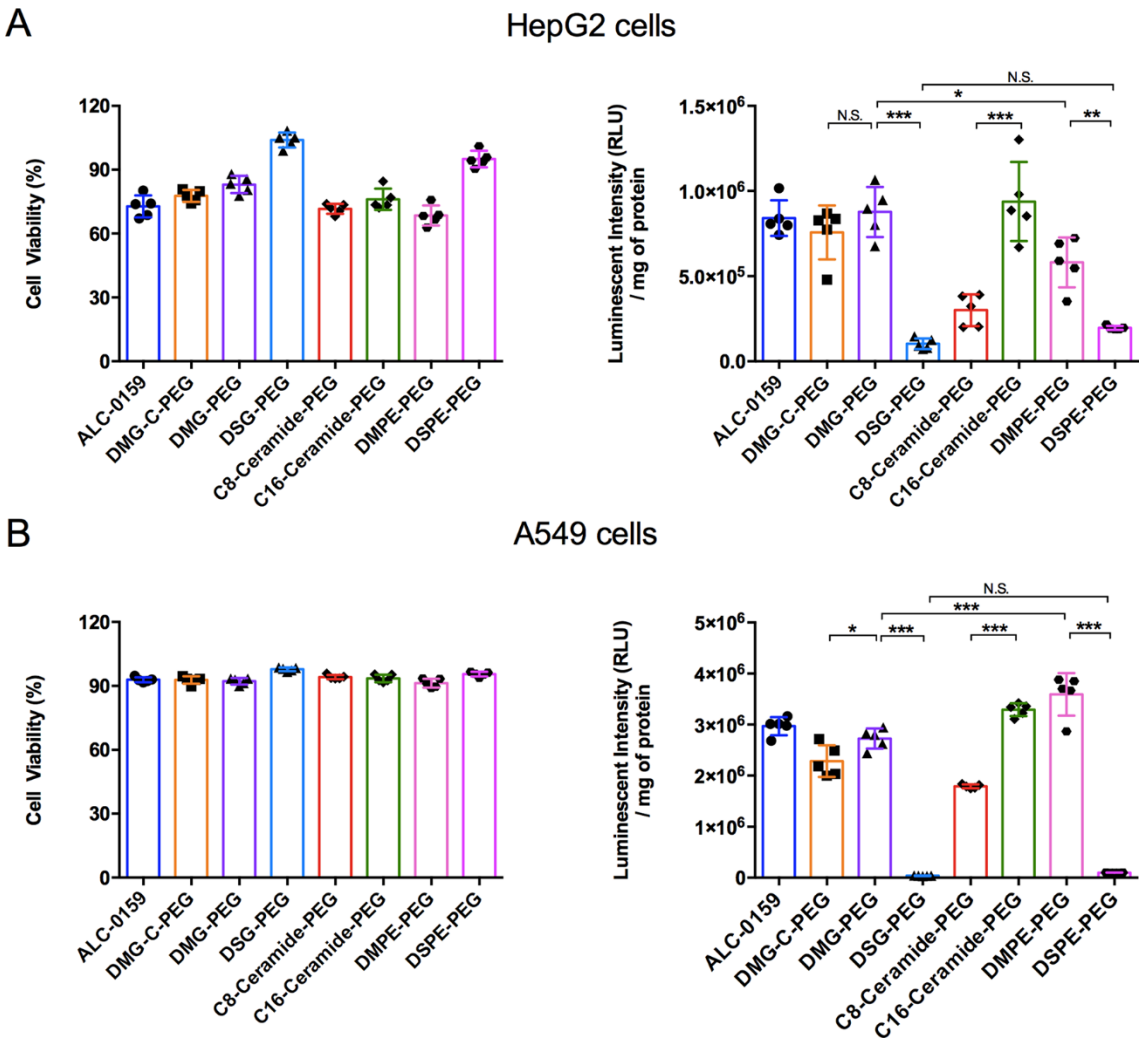

Figure 6. Cytocompatibility and normalized translation efficiency of FLuc mRNA-LNPs prepared with different PEG-lipids at 1.6% molar content *via* microfluidic mixing in HepG2 (A) and A549 (B) cells. (n = 5 per group).

3.4 Membrane fusion of mRNA-LNPs

The RBCs hemolysis assay was employed to investigate the membrane fusion activity of mRNA-LNPs at endosomal pH (5.5 and 6.5) due to the lipid bilayer similarities between RBCs and endosomes [34]. We also assessed the hemolytic activity of the mRNA-LNPs at physiological pH (pH 7.4) to study their compatibility with RBCs. As shown in **Figure 7A**, the hemolysis rate of the mRNA-LNPs at pH 7.4 was below 2.5 %, indicating good compatibility of the LNPs with the RBCs. This result aligns with the observed cytotoxicity profiles in the tested cell lines (**Figures 4**, **6 & 10**). A similar phenomenon was also observed for mRNA-

LNPs at pH 6.5. However, the hemolysis rate under pH 5.5 was significantly higher. LNPs formulated with C8-Ceramide-PEG showed the highest hemolysis rate, which was 65.8 ± 1.0 %. LNPs formulated with ALC-0159, or C16-Ceramide-PEG showed moderate hemolysis rates, both of which were around 25 %. In contrast, LNPs formulated with DSPE-PEG showed the lowest hemolysis rate, which was 15.9 ± 0.3 % under pH 5.5. These results indicated that the LNPs formulated with C8-Ceramide-PEG had the highest capability to destabilize and escape endosomes through membrane fusion while LNPs formulated with DSPE-PEG had the lowest capability.

3.5 Surface ionization property and serum stability of mRNA-LNPs

The apparent pKa value of LNPs formulated with C8-Ceramide-PEG, ALC-0159, and C16-Ceramide-PEG was comparable, ranging from 6.16 to 6.13. The pKa value (5.94) of LNPs formulated with DSPE-PEG was lower, especially when compared with the LNPs prepared from C8-Ceramide-PEG (**Figures 7B & 7C**). The relatively lower pKa value of DSPE-PEG LNPs might be a reason for the lower mRNA translation efficiency (**Figure 6**).

When the LNPs were incubated with 10 % FBS, the size of LNPs formulated with ALC-0159, C16-Ceramide-PEG, and DSPE-PEG was stable during the period of 48 h (**Figures 7D & 7E**). However, the size of LNPs formulated with C8-Ceramide-PEG increased from 70.6 ± 0.5 nm to 113.3 ± 0.8 nm. The PDI and zeta potential of the four mRNA-LNPs remained relatively stable during the incubation of 48 h (**Figure S3**). These results indicated that C8-Ceramide-PEG with a shorter lipid tail affect the serum stability of mRNA-LNPs.

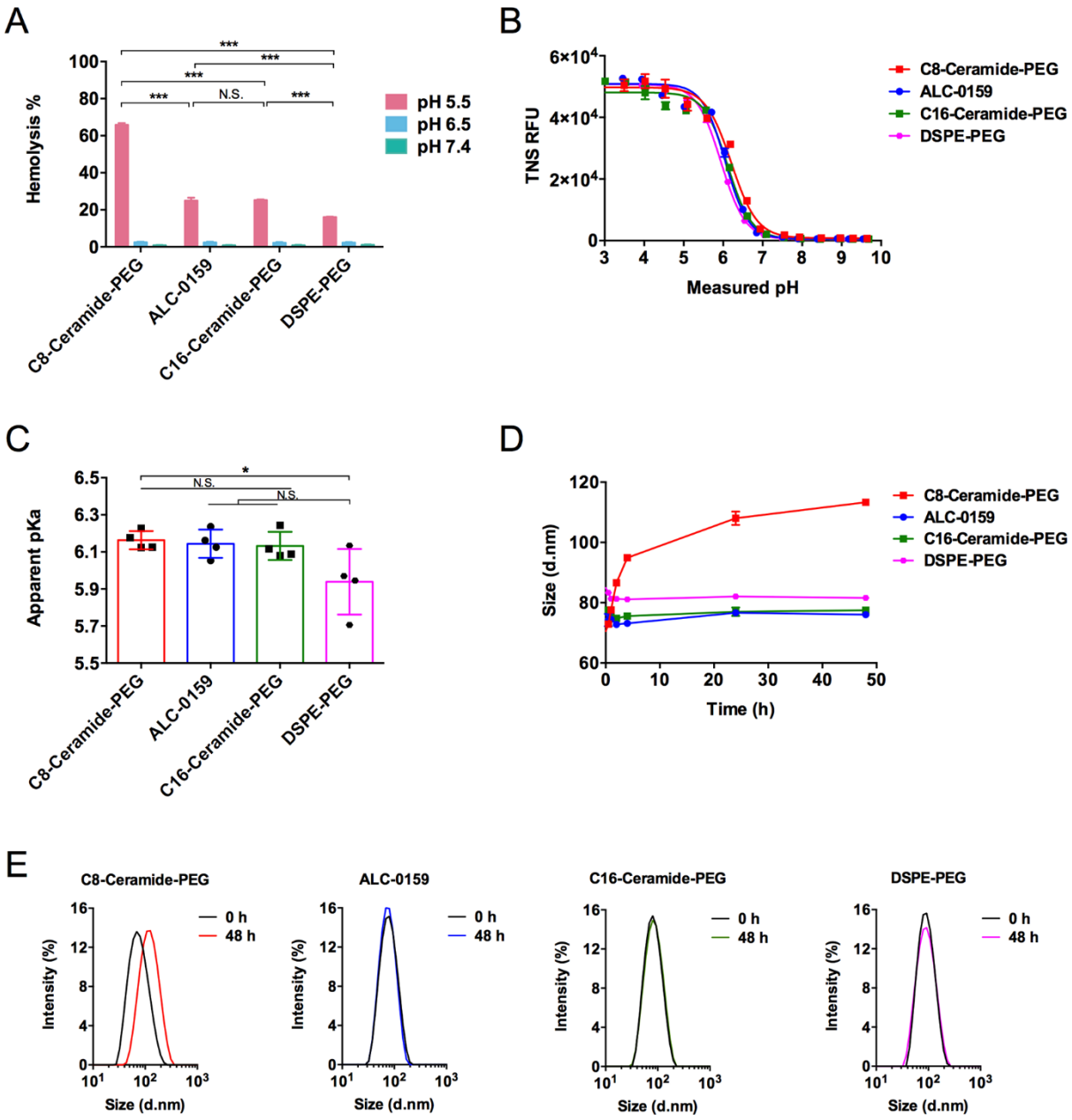

Figure 7. Hemolysis, pKa, and serum stability of mRNA-LNPs. (A) Hemolysis activity of mRNA-LNPs under different pH conditions. (B) Representative TNS binding assay curves. (C) apparent pKa values of mRNA-LNPs tested by the TNS binding assay. (D) Size changes and (E) Size distribution profiles of mRNA-LNPs incubated in PBS containing 10% FBS at different time points. (*n* = 3-4 per group).

3.6 In vitro cellular uptake and endosomal escape of mRNA-LNPs

Mechanistic insights into mRNA delivery were explored through confocal live cell imaging in HepG2 cells (**Figure 8**). The cellular uptake of ALC-0159 and C16-Ceramide-PEG LNPs was higher than that of C8-Ceramide-PEG and DSPE-PEG LNPs. The lower cellular uptake of C8-

Ceramide-PEG LNPs was likely attributed to their reduced stability in the presence of serum as shown in **Figure 7D & 7E**. In addition, DSPE-PEG LNPs exhibited lower endosomal escape efficiency than ALC-0159 and C16-Ceramide-PEG LNPs, which was consistent with membrane fusion results shown in **Figure 7A**. However, C8-Ceramide-PEG LNPs showed lower endosomal escape efficiency, which contradicted the membrane fusion results. One possible explanation for the discrepancy is the absence of serum in the membrane fusion study. The aggregation of C8-Ceramide-PEG LNPs in the presence of serum might compromise their endosomal escape. The lower cellular uptake and endosomal escape efficiency of C8-Ceramide-PEG and DSPE-PEG LNPs contributed to lower mRNA translation efficiency in cells (**Figure 6**).

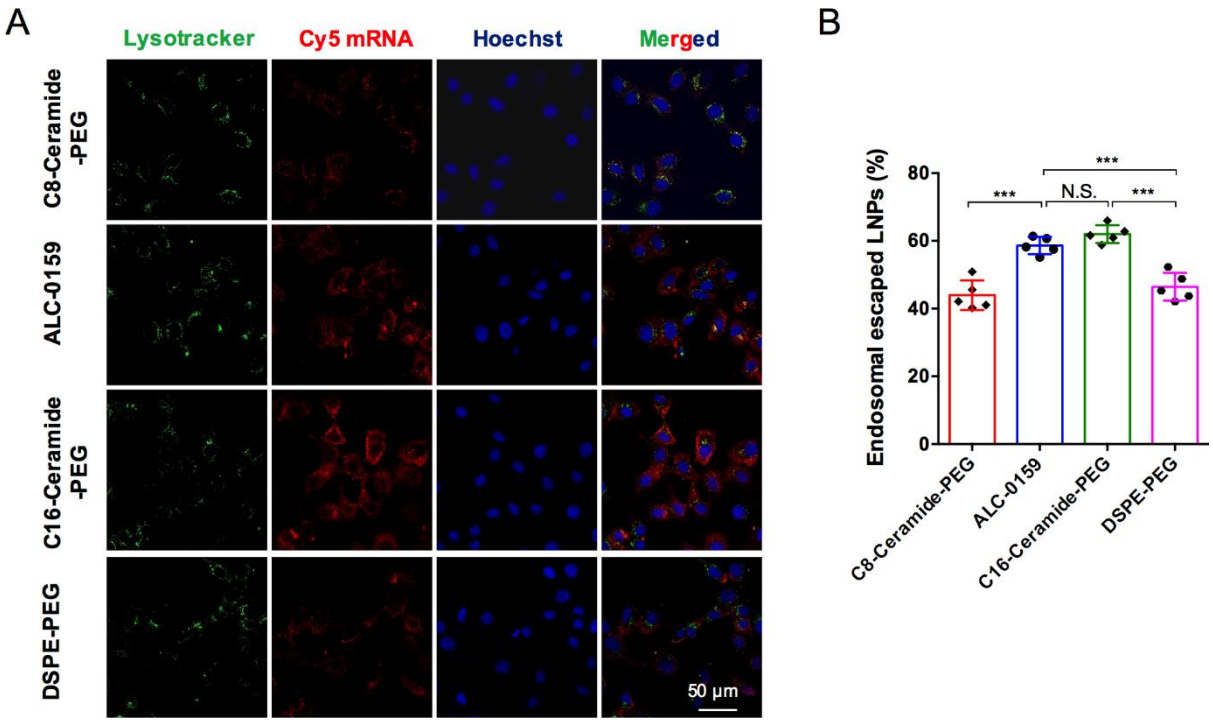

Figure 8. Study of cellular uptake and endosomal release of Cy5-labeled mRNA-LNPs after 6 h of incubation with HepG2 cells. (A). Representative confocal laser scanning microscopic images. Blue, green, and red fluorescent regions indicate nuclei, endo-lysosomes of cells, and Cy5-labeled mRNA-LNPs, respectively. The scale bar represents 50 μm. (B) Percentage of Cy5-labeled mRNA-LNPs escaped from the endo-lysosomes, calculated using Image J software. (n = 5 per group).

3.7 In vivo protein expression of FLuc mRNA-LNPs

The *in vivo* protein expression study was performed using Fluc mRNA-LNPs made from the selected PEG-lipids *via* microfluidic mixing to investigate their impact on *in vivo* behavior of mRNA-LNPs. At 6 h post-injection, strong bioluminescence signal was seen in the injection area (skin), liver, and lymph nodes (overlapping or distinct signal sites around the injection area) from the whole body images (**Figure 9A-9C**), indicating all mRNA-LNPs successfully mediated *in vivo* mRNA transfection. The mRNA-LNPs made from C8-Ceramide-PEG were mainly accumulated in the injection site and lymph node with minimal accumulation in the liver, whereas mRNA-LNPs prepared from ALC-0159 and C16-Ceramide-PEG were largely accumulated in the liver and skin. Among all LNPs tested, the mRNA-LNPs made from DSPE-PEG with the longest lipid tails yielded the lowest *in vivo* transfection efficiency at 6 h. This finding is in agreement with the *in vitro* results (**Figure 6**). The signal declined at 24 h post-injection.

From the *ex vivo* images of the collected organs/tissues (**Figure S4**), all LNPs tested had comparable luciferase expression. The primary signal accumulation was observed in the liver, lymph node, and skin (**Figures 9D & S4C**). No significant difference in the signal of lymph node was observed across the four LNPs-treated groups. C8-Ceramide-PEG LNPs induced significantly lower luciferase expression in the liver than C16-Ceramide-PEG LNPs (**Figure 9D**). ALC-0159 LNPs yielded significantly higher luciferase expression in the skin, i.e., 16.37-, 18.55-, and 8.93-fold as compared to C8-Ceramide-PEG, C16-Ceramide-PEG, and DSPE-PEG LNPs, respectively. From the analysis of organ/tissue specificity (**Figure 9E**), mRNA-loaded C16-Ceramide-PEG LNPs showed the highest liver specificity while C8-Ceramide-LNPs showed the lowest liver specificity compared to the rest organs/tissues. The accumulation of mRNA-loaded ALC-0159 LNPs in the liver, lymph node, and skin was comparable. DSPE-PEG LNPs demonstrated a higher lymph node specificity than ALC-0159 and C16-Ceramide-

PEG LNPs, comparable to C8-Ceramide-PEG LNPs (**Figure 9E**). Therefore, the lipid tail length of PEG-lipids significantly affected the protein expression of subcutaneously administered mRNA-LNPs, particularly at the liver, injection area, and lymph node.

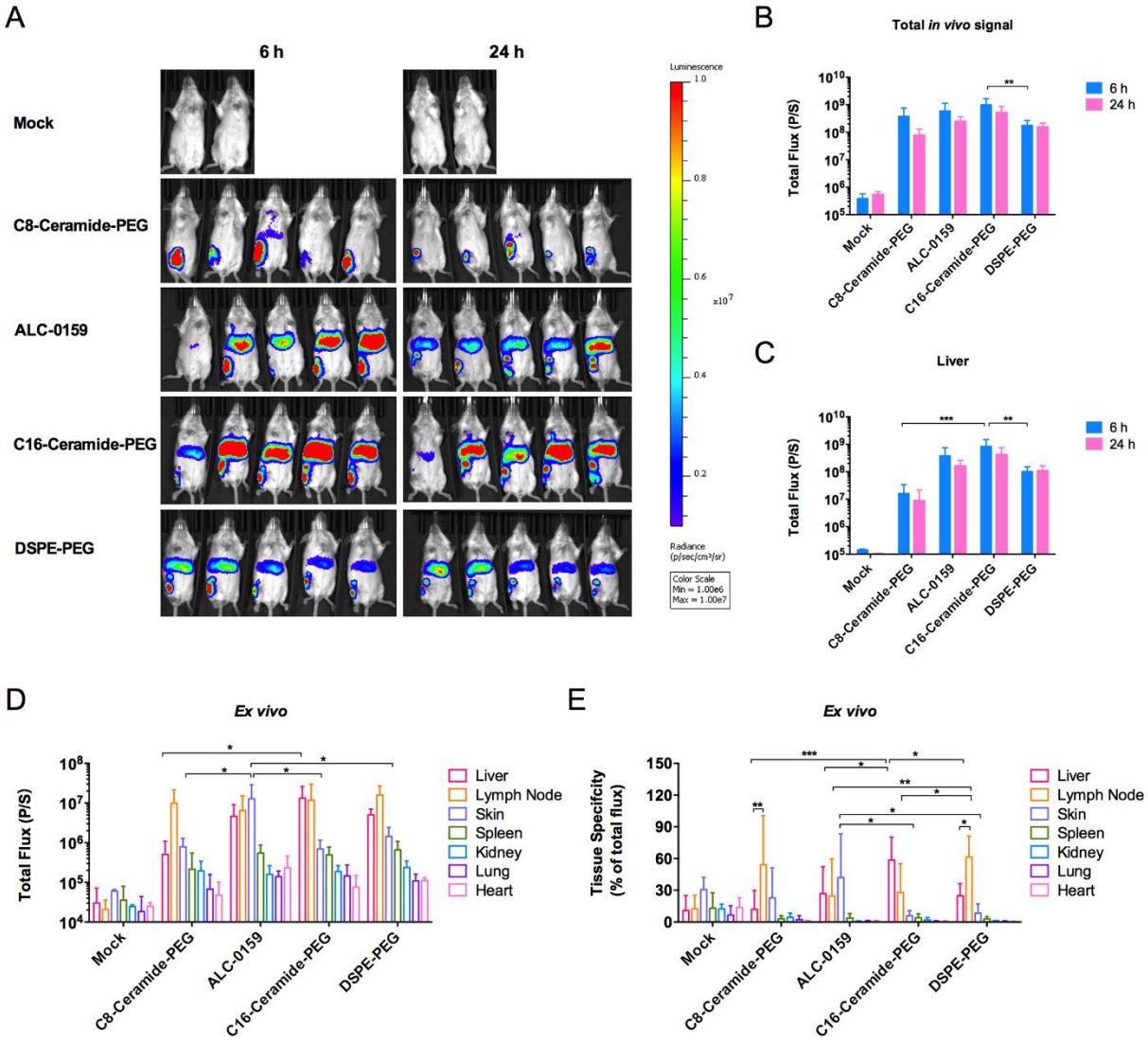

Figure 9. *In vivo* protein expression of FLuc mRNA-LNPs formulated *via* microfluidic mixing. (A) Bioluminescence images of BALB/c mice at 6 and 24 h after s.c. administration of Fluc mRNA-LNPs. (B) Total flux of the whole body quantified from the bioluminescence images at 6 and 24 h after s.c. adminstration. (C) Total flux of the liver quantified from the bioluminescence images at 6 and 24 h after s.c. administration. (D&E) *Ex vivo* total flux of each collected organ/tissue (D) and tissue specificity (E) at 24 h post administration. (n = 2-5 per group).

3.8 In vitro study of LNPs loaded with mRNA encoding spike protein of SARS-CoV-2 Delta variant

Furthermore, mRNA encoding the spike protein of SARS-CoV-2 Delta variant was loaded into the LNPs *via* microfluidic mixing. The average size of resulting LNPs is slightly larger than FLuc mRNA-LNPs (**Figures 5 & S5**), which was likely attributed to the difference in mRNA length (mRNA encoding spike protein of SARS-CoV-2 Delta variant: close to 4000 nucleotides; FLuc mRNA: 1922 nucleotides). LNPs formulated with C8-Ceramide-PEG and ALC-0159 had an average size of around 80 nm, whereas the size of LNPs with C16-Ceramide-PEG and DSPE-PEG were 90.1 ± 1.0 and 111.2 ± 0.3 nm, respectively (**Figure S5**). The encapsulation efficiency of LNPs loaded with SARS-CoV-2 Delta spike protein encoded mRNA was relatively higher than that of LNPs loaded with FLuc mRNA, whereas their PDI and zeta potential were comparable (**Figures 5 & S5**).

All LNPs loaded with mRNA encoding spike protein of SARS-CoV-2 Delta variant showed negligible cytotoxicity towards both HepG2 and A549 cells with cell viability higher than 90 % (**Figure 10A & 10B**). The spike protein expression mediated by mRNA-LNPs was cell type-dependent, being higher in A549 cells (**Figure 10A & 10B**). Among all LNPs, mRNA-loaded ALC-0159 LNPs yielded the highest spike protein expression, while the lowest spike protein expression was induced by mRNA-loaded DSPE-PEG LNPs especially in HepG2 cells. There was no significant difference in the spike protein expression between LNPs formulated with C8-Ceramide-PEG and C16-Ceramide-PEG in both cell lines.

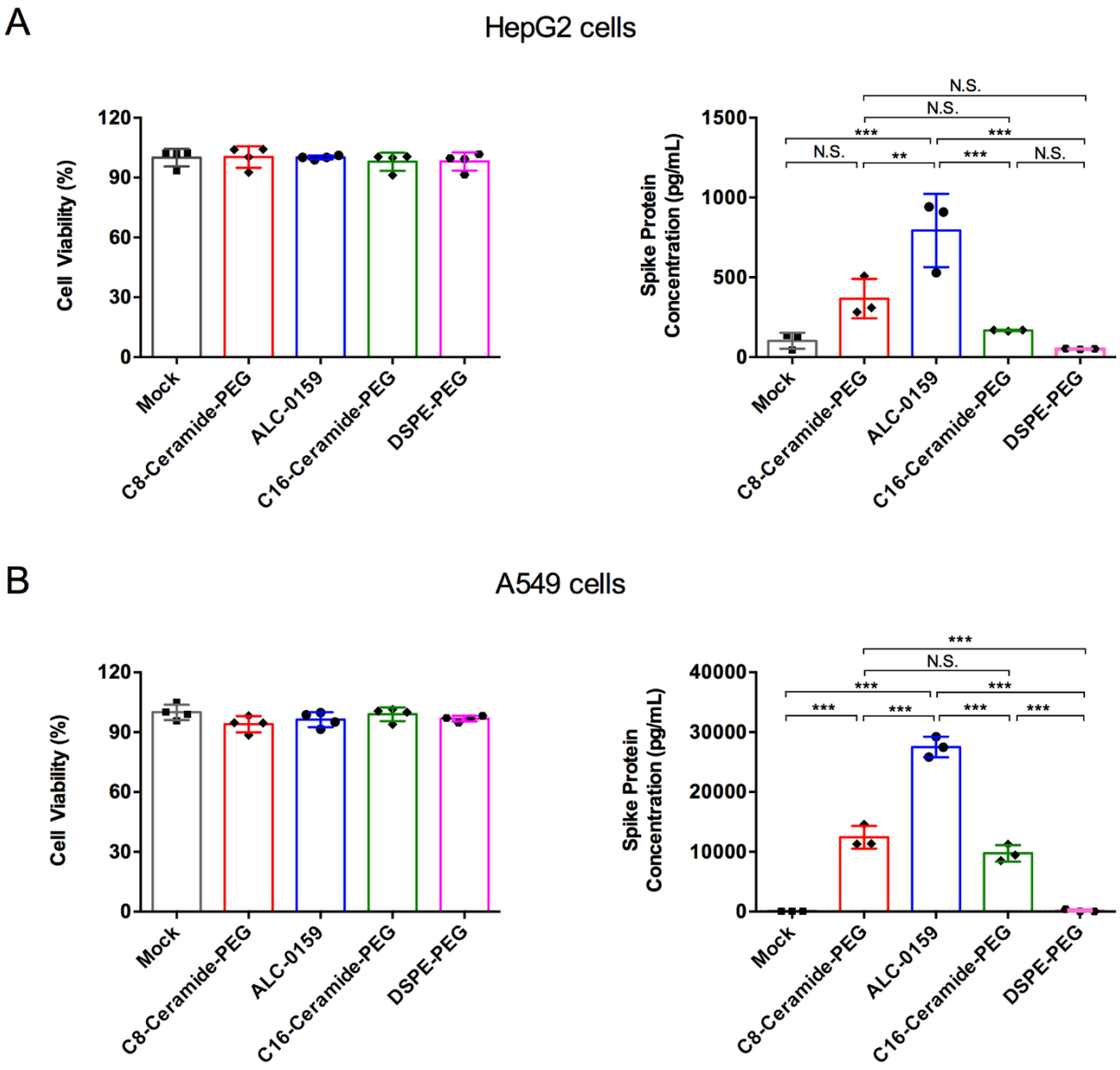

Figure 10. Cytocompatibility of and spike protein expression mediated by LNPs loaded with mRNA encoding spike protein of SARS-CoV-2 Delta variant, prepared with different PEG-lipids at 1.6% molar content *via* microfluidic mixing in HepG2 (A) and A549 (B) cells. (n = 3-4 per group).

3.9 In vivo immunogenicity of LNPs loaded with mRNA encoding spike protein of SARS-CoV-2 Delta variant

To evaluate their immunogenicity, LNPs loaded with mRNA encoded for Delta variant spike protein were administrated into mice subcutaneously (**Figure 11A**). Throughout the experiment, no sign of weight loss was observed, indicating the safety of the LNPs (**Figure 11B**). After the 1st dose, LNPs formulated with DSPE-PEG showed significantly lower ability

to block RBD-ACE2 interaction, suggesting less production of neutralizing antibodies than other LNPs. This is in agreement with the *in vitro* results (**Figure 10**). The trend maintained until week 3, with only 29.9 ± 10.8% inhibition (**Figure 11C**). In contrast, the other three treated groups had inhibition of around 60 % from week 1 to 3, with no significant difference among them. One week after the 2nd dose, the inhibition of the four treated groups dramatically increased to > 90 % and maintained high until week 11.

The treated mice also produced notable levels of IgG antibodies against spike protein (**Figure 11D**), following a similar trend with the results of RBD-ACE2 interaction blocking. However, at the endpoint, mRNA-LNPs formulated with DSPE-PEG displayed significantly lower anti-spike IgG endpoint titer than those prepared with ALC-0159. No significant difference was observed among the groups treated with mRNA-LNPs made from C8-Ceramide-PEG, C16-Ceramide-PEG, and ALC-0159, respectively. These results indicated that LNPs formulated with these PEG-lipids were able to induce immunogenicity in mice. However, mRNA-LNPs made from DSPE-PEG showed lower production of neutralizing and anti-spike IgG antibodies than mRNA-LNPs prepared from the other PEG-lipids, and the anti-spike IgG antibody generated by mRNA-LNPs made from DSPE-PEG declined faster than mRNA-LNPs made from ALC-0159. The production of IgG antibodies against spike protein and effective RBD-ACE2 interaction blocking proves activation of B cells.

The production of anti-PEG antibody was investigated after vaccination as well. The mRNA-LNPs formulated with DSPE-PEG showed a peak anti-PEG IgM level at week 1 post-1st dose, followed by a gradual decrease until week 3 (**Figure 11E**). A second peak was observed one week after the boost dose, then gradually decreased again to a comparable level with the Mock group. In addition, LNPs formulated with C16-Ceramide-PEG induced anti-PEG antibody

response at one week after the boost dose, while LNPs formulated with C8-Ceramide-PEG or ALC-0159 maintained anti-PEG IgM levels comparable to the Mock group throughout the experiment. In contrast, the anti-PEG IgG levels in all treated groups were much lower than anti-PEG IgM levels throughout the experiment (**Figure 11F**). The LNPs formulated with DSPE-PEG only showed a slightly higher anti-PEG IgG level than the other LNPs and no significant difference observed. Therefore, these results showed that the lipid tail length in PEG-lipid significantly affected the induction of anti-PEG antibody by mRNA-LNPs. With C8-Ceramide-PEG and ALC-0159 used in mRNA-LNPs, the levels of anti-PEG antibody induced were negligible.

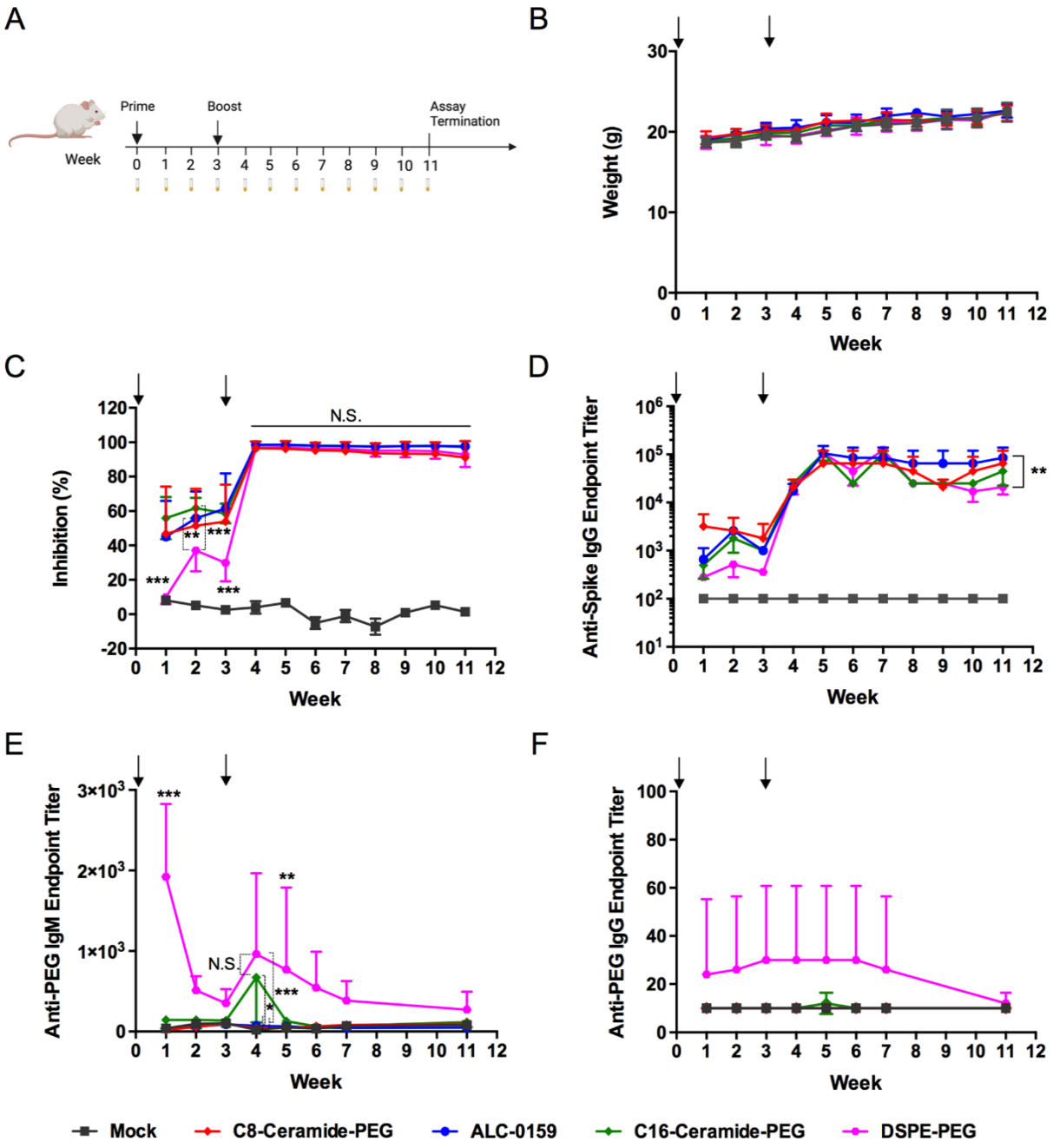

Figure 11. *In vivo* immunogenicity activity of LNPs loaded with mRNA encoded for SARS-CoV-2 Ddelta variant spike protein in BALB/c mice. (A) Timeline and treatment course of the immunogenicity study. (B) Body weight change of all groups throughout the experimental period. (C) ACE2-RBD binding inhibition of the sera from each group during the whole experiment period. (D-F) Anti-spike IgG titers (D), anti-PEG IgM titers (E), and anti-PEG IgG titers (F) of the sera from each group during the experimental period. The arrows indicated prime and boost injection of the LNPs. (n = 5 per group; N.S., no significant difference; * p < 0.05; ** p < 0.01; and *** p < 0.001 between two indicated groups or the DSPE-PEG treated group with the rest three treated groups).

The treatment with the mRNA-LNPs showed no significant alteration in toxicity markers for the liver (albumin, ALP, ALT, and total protein), heart (CK-MB), and kidney (creatinine and

urea) [35] compared to the Mock group (**Figure 12**), further demonstrating the safety profile of LNPs. Nevertheless, the quantification of creatinine level in LNPs prepared with C16-Ceramide-PEG and DSPE-PEG was higher than that in LNPs prepared with C8-Ceramide-PEG and ALC-0159. The results suggest that the treatment with the mRNA-LNPs formulated with C8-Ceramide-PEG, ALC-0159, C16-Ceramide-PEG, or DSPE-PEG did not induce obvious hepatic-, renal-, or cardio- toxicity in the treated mice.

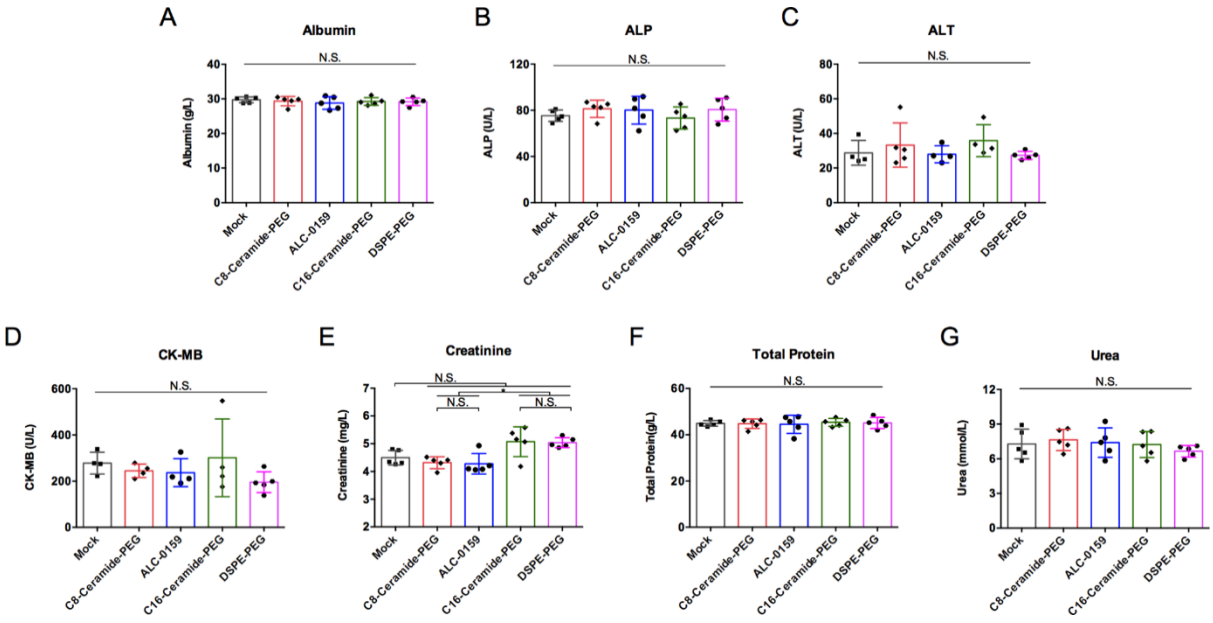

Figure 12. Blood biochemical analysis including albumin (A), ALP (B), ALT (C), CK-MB (D), creatinine (E), total protein (F), and urea (G) in BALB/c mice treated with LNPs loaded with mRNA encoded for SARS-CoV-2 Delta variant spike protein at the endpoint of *in vivo* immunogenicity experiment. (n = 4-5 per group; The outliers were determined using Grubb's test and removed from the data analysis).

4. Discussion

In this study, different parameters of PEG-lipid including molar content, chemical linkage between PEG and lipid tails, lipid tail length, LNP preparation techniques, and mRNA size were investigated to explore the impact of PEG-lipid on the performance of mRNA-LNPs. PEG-lipid with a PEG molecular weight of 2000 Da showed the best equilibrium between anti-opsonization and *in vivo* delivery efficacy [36]. Longer PEG chains were associated with higher allergic risk [21]. Taken together, PEG-lipids with PEG of 2000 Da were chosen in this study.

The size of mRNA-LNPs influences vaccine delivery efficacy. For viruses including SARS-CoV-2, influenza A, and HIV, the size of nanoparticulate vaccines of around 100 nm is optimal for high immunogenicity [37]. One study reported that increasing the PEG molar ratio from 1.0 to 5.0 % reduced the average size while keeping the PDI below 0.2 [14]. A similar trend was observed in our study for mRNA-LNPs made from most of the PEG-lipids. However, unlike the other PEG-lipids tested in this study, increasing the content of DSPE-PEG with C18 lipid tails led to mRNA-LNPs with significantly larger particles and higher PDI (**Figures 3A&3B**). The exact reason behind this phenomenon is unclear, but it might be related to interactions between the lipid tails of PEG-lipid and shell-forming lipids, and the packing dynamics of the four lipids. Longer alkyl chains in PEG-lipid may contribute to higher hydrophobic interactions, possibly resulting in more compact LNPs. This phenomenon was not observed in this study. The larger sizes of DSPE-PEG and C16-Ceramide-PEG LNPs compared to their shorter-tailed counterparts (DMPE-PEG and C8-Ceramide-PEG, respectively) may result from differences in the packing dynamics of the four lipids during the self-assembly process. This suggests that factors beyond hydrophobic interactions, such as lipid packing behavior and overall structural organization, play a role in determining LNP size. Microfluidic mixing produced mRNA-LNPs had sizes below or around 100 nm, smaller than those prepared *via* manual mixing (**Figure 5A**). The size decrease of LNPs from manual mixing to microfluidic mixing was also observed previously [38]. The reason was that microfluidic mixing gave more time and offered more homogenous mixing for the lipids and mRNA to self-assemble into more compact mRNA-LNPs. mRNA with a bigger size formed slightly larger LNPs especially for DSPE-PEG likely because more ionizable lipids were needed to condense the mRNA into LNPs, increasing particle size.

Cholesterol was in a crystalline form on the surface of LNPs to increase the membrane rigidity, preventing the leakage of payload from the core [39, 40]. However, increasing the PEG-lipid content reduces the cholesterol content in the LNP formulation, potentially compromising the membrane rigidity and cargo retention. This reduction in structural integrity leads to a decline in encapsulation efficiency. Specifically, the encapsulation efficiency of mRNA dropped significantly below 50 % when PEG-lipid molar content exceeded 3.0 % (**Figure 3D**). The variations in the size and encapsulation efficiency indicated that achieving the desired properties of LNPs depended on the lipid tail length of PEG-lipid, PEG-lipid molar ratio, and the preparation technique.

PEG-lipid also affected mRNA translation efficiency *in vitro*. The chemical linker between PEG and lipid tail showed limited influences in mRNA translation efficiency (**Figure 4**). However, increasing the content of PEG-lipid greatly reduced the translation efficiency in both HepG2 and A549 cell lines. This trend was consistent with another study reported previously due to the inhibition of endosomal release of mRNA and interference with cellular uptake at high molar ratios of PEG-lipid [41]. In addition, the length of lipid tail in PEG-lipid played a crucial role in mediating mRNA translation. DSG-PEG and DSPE-PEG with C18 lipid tails induced significantly lower translation efficiency than their counterpart (DMG-PEG and DMPE-PEG, respectively), while a reversed trend was observed for C8-Ceramide-PEG and C16-Ceramide-PEG LNPs formulated *via* microfluidic mixing (**Figure 6**). Previous studies demonstrated that LNPs prepared using PEG-lipids containing longer carbon tails exhibited lower *in vitro* mRNA translation efficiency compared to those with shorter carbon tails, even using a different ionizable lipid such as DLin-MC3-DMA [28]. These findings further confirmed the effect of lipid carbon length of PEG-lipids on the delivery potency of LNPs, regardless of the specific ionizable lipid employed.

Moreover, the size of mRNA payload is another factor that influences *in vitro* mRNA transfection. When mRNA encoded for SARS-CoV-2 Delta variant spike protein with a larger size was used, there was no significant difference in the translation efficiency between LNPs formulated with C8-Ceramide-PEG and C16-Ceramide-PEG in both HepG2 and A549 cell lines (**Figure 10**). Additionally, ALC-0159 yielded significantly greater translation efficiency than C16-Ceramide-PEG, while such a trend was not observed when FLuc mRNA with a smaller size was employed. The impact of mRNA size on the protein translation efficiency of mRNA-LNPs was also reported by K. Mrksich et al. [42]. Furthermore, the preparation method also affected translation efficiency. When the microfluidic technique was used to fabricate FLuc mRNA-loaded LNPs, the transfection efficiency was higher than those prepared by manual mixing, especially for ALC-0159 LNPs (**Figures 4 & 6**). This might be because sufficient mixing time and homogenous mixing produced well-assembled LNPs, which potentially facilitated fusion with endosomal membrane and endosomal release. Since the preparation method affected packing of lipids, it changed the trends that we observed especially for C8-Ceramide-PEG and C16-Ceramide-PEG.

The pKa value of LNPs is crucial to high transfection efficiency, with an ideal pKa range of 6.2 to 6.5 for mRNA-LNPs [43]. SM-102 and ALC-0315 lipids exhibited pKa value of 6.68 and 6.09, respectively [44]. The apparent pKa value of ALC-0315 LNPs made from DMG-PEG was reported to be 6.27 at N/P 5 [45], indicating that the apparent pKa of LNPs is different from that of the ionizable lipid and affected by the packing. Although mRNA-LNPs made with C8-Ceramide-PEG, C16-Ceramide-PEG, or DSPE-PEG have a comparable pKa value as those made with ALC-0159 (**Figures 7B & 7C**), the use of C8-Ceramide-PEG or DSPE-PEG yielded significantly lower mRNA translation efficiency (**Figures 6A & 6B**). This reduction is

attributed to the lower cellular uptake and endosomal release efficiency of C8-Ceramide-PEG or DSPE-PEG LNPs (**Figure 8**).

For effective vaccination, delivering mRNA to lymph nodes is crucial because they are command centers of the immune response, housing T cells, B cells, and antigen-presenting cells (APCs) [46]. LNPs smaller than 200 nm could be drained to lymph nodes *via* lymphatics at the site of injection [47, 48]. Previous research has shown that decreasing PEG content increased the total flux of FLuc mRNA-LNPs in mice, highlighting the impact of PEG-lipid on *in vivo* mRNA delivery [22, 28]. Subcutaneous injection typically results in slow absorption and the signal at the injection site could last several days due to relatively low irrigation (vascular density) [49, 50]. Thus, it is not surprising that the signal of FLuc mRNA-LNPs was observed at the injection site after 6 h of injection. After subcutaneous injection, partial LNPs can migrate to the nearest draining lymph node, where immunization occurs [46].

The adsorption of apolipoprotein E (ApoE) on circulating LNPs upon PEG-lipid shedding could drive the LNPs to hepatocytes, resulting in a high bioluminescence signal in the liver [40]. Once LNPs enter blood circulation, PEG-lipids on the surface of LNPs begin to shed. Previous studies have shown that PEG-lipids with longer carbon alkyl tails tend to shed more slowly than those with shorter tails [29]. For example, a pharmacokinetics study revealed that the shedding rates for C14, C16, and C18 PEG-lipids at the molar ratio of 1.5 % were 45 %, 1.3 %, and 0.2 % per hour, respectively, regardless of the chemical linkage type between PEG and lipids moieties [51]. This shedding behavior was consistent across various formulations, including siRNA-LNPs and PLGA nanoparticles [19, 52]. Based on these findings, C8-Ceramide-PEG is expected to shed faster than ALC-0159 from the surface of LNPs. This is supported by another pharmacokinetics study where C8-Ceramide-PEG liposomes exhibited

the fastest clearance from blood circulation compared with C14- to C20-Ceramide-PEG liposomes when administrated *via* tail vein injection [53]. Rapid clearance and poor stability of C8-Ceramide-PEG LNPs in a serum-containing medium likely reduce liver accumulation, as seen in our study (**Figure 9**), in contrast to LNPs containing ALC-0159, C16-Ceramide-PEG, or DSPE-PEG. However, C8-Ceramide-PEG LNPs may follow a different biodistribution pattern upon subcutaneous administration, potentially draining *via* lymphatics to lymph nodes upon subcutaneous injection [48] as suggested by **Figure 9**. The lower bioluminescence signal in the liver, mediated by LNPs formulated with DSPE-PEG compared to C16-Ceramide-PEG at 6 h (**Figure 9C**) could be caused by the lower mRNA translation efficiency (**Figure 6**).

Although a previous study demonstrated that PEG-lipids with lipid tail length shorter than C12 exhibited negligible efficacy compared to C13 to C15 in lipid-siRNA formulations[54], our results suggest that the mRNA-LNPs formulated with C8-Ceramide-PEG achieve comparable RBD-ACE2 interaction inhibition, and notable anti-spike IgG titer levels, comparable to those mediated by the mRNA-LNPs formulated with ALC-0159 (**Figure 11**). While C8-Ceramide-PEG LNPs showed lower *in vitro* mRNA translation efficiency than ALC-0159 LNPs (**Figure 10**), the comparable vaccination efficacy observed *in vivo* could be attributed to the enhanced lymph node targeting of C8-Ceramide-PEG LNPs (**Figure 9**). Furthermore, the reduced liver accumulation of C8-Ceramide-PEG LNPs indicates a potentially lower risk of hepatotoxicity of the LNPs. This property could offer significant advantages for high-dose or repeated-dose administrations [55], which is a common scenario for mRNA vaccine delivery. Thus, while the improved lymph node targeting did not translate to a dramatic enhancement in vaccine efficacy compared to ALC-0159, C8-Ceramide-PEG LNPs provide a promising alternative with a potentially favorable safety profile.

PEGylation of LNPs is known to trigger the generation of anti-PEG antibodies, leading to the accelerated blood clearance (ABC) effect [56]. The produced anti-PEG antibodies could also trigger the complement activation-related pseudoallergy (CARPA), leading to adverse effects [57]. Due to these concerns, the US FDA recommends monitoring anti-PEG antibodies to ensure the safety of PEGylated products [57]. Studies have shown PEG-lipids with slower shedding rates were associated with higher production of anti-PEG IgM antibodies. In this study, the production of anti-PEG IgM level showed a positive correlation with the length of the lipid tail in PEG-lipid, which was agreeable with a previous study despite differences in the payload and formulation [19]. This is likely attributed to the slow shedding rate of DSPE-PEG and C16-Ceramide-PEG, due to their long alkyl chains. This prolonged retention of DSPE-PEG and C16-Ceramide-PEG on the LNP surface might lead to extended circulation and increased exposure to splenic marginal zone B cells, which are responsible for producing anti-PEG antibodies. The variation of anti-PEG IgM level demonstrated a minimum two-week dose interval may be necessary for LNPs formulated with PEG-lipid containing intermediate or long lipid tails (e.g., C16 and C18) as the level of anti-PEG antibodies dropped back to the baseline 2-3 weeks post-1st vaccination dose. The negligible anti-PEG IgM level after the treatment with the mRNA-LNPs formulated with C8-Ceramide-PEG and ALC-0159 could be explained by the relatively low dose of mRNA-LNPs applied and the administration route (**Figure 11E**) [58, 59].

5. Conclusions

Our study revealed chemical linkages between PEG and lipid tails of PEG-lipid such as carbamate and phosphate had a limited impact on physicochemical properties and translation efficiency of mRNA-LNPs, while PEG-lipid molar content and lipid tail length played crucial

roles. An increased PEG-lipid molar content led to a reduction in particle size, encapsulation efficiency, and mRNA translation efficiency for the majority of the PEG-lipids studied. However, for DSPE-PEG with C18 lipid tails, an increased PEG content yielded larger particle size and wider size distribution. DSG-PEG and DSPE-PEG with C18 lipid tails led to significantly lower *in vitro* mRNA translation efficiency than DMG-PEG and DMPE-PEG with C14 tails, respectively. However, when compared with C8-Ceramide-PEG, C16-Ceramide-PEG with a longer tail produced FLuc mRNA-LNPs with greater *in vitro* translation efficiency when microfluidic mixing was employed. The FLuc mRNA-LNPs formulated with C8-Ceramide-PEG showed lower liver accumulation but comparable protein expression at the lymph nodes when compared with those formulated with ALC-0159 or C16-Ceramide-PEG. In a mouse model, the SARS-CoV-2 Delta variant spike protein-encoded mRNA-LNPs prepared with C8-Ceramide-PEG or C16-Ceramide-PEG achieved comparable vaccination efficacy to ALC-0159, while the mRNA-LNPs prepared from DSPE-PEG with C18 tails induced lower vaccination efficacy. In addition, C16-Ceramide-PEG and DSPE-PEG LNPs mediated higher anti-PEG IgM titers in mice than C8-Ceramide-PEG and ALC-0159 LNPs. The use of these PEG-lipids in mRNA-LNPs did not cause any significant toxicity in mice. These findings provide insights into the utilization of PEG-lipids in LNP formulation for mRNA vaccine delivery. With their ability to target lymph nodes, low risk of hepatotoxicity, high vaccination efficacy and negligible anti-PEG antibody response, C8-Ceramide-PEG LNPs emerge as a promising alternative for mRNA vaccine delivery.

Acknowledgements

This study was financially supported by the Bioprocessing Technology Institute (BTI), Biomedical Research Council (BMRC), Agency for Science, Technology and Research (A*STAR), IAF-PP (H22J1a0050) and NRF-CRP (CRP27-2021-0038), Republic of Singapore.

CRediT authorship contribution statement

Li Zhang - Conceptualization, Data curation, Methodology, Formal analysis, Writing-original draft, Writing-review & editing. **Brandon Yi Loong Seow -** Data curation, Formal analysis, Methodology, Writing-review & editing. **Ki Hyun Bae** - Data curation, Formal analysis, Methodology, Writing-review & editing. **Yue Zhang** - Data curation, Formal analysis, Methodology, Writing-review & editing. **Kuo-Chieh Liao** - mRNA synthesis, Writing-original draft, Writing-review & editing. **Yue Wan -** Visualization, Supervision, Writing-review & editing. **Yi Yan Yang** - Conceptualization, Supervision, Formal analysis, Writing-review & editing, Funding acquisition. All authors have given approval to the final version of the manuscript.

Appendix A. Supplementary data

Supplementary material to this article can be available online at https://doi.org/10.1016/j.jconrel.2025.01.071.

Declaration of competing interest

The authors declare no conflict of interest.

Data availability

The relevant data will be provided with a reasonable request.

References

[1] E.L. Han, M.S. Padilla, R. Palanki, D. Kim, K. Mrksich, J.J. Li, S. Tang, I.C. Yoon, M.J. Mitchell, Predictive high-throughput platform for dual screening of mRNA lipid nanoparticle blood-brain barrier transfection and crossing, Nano Lett. 24 (2024) 1477-1486. https://doi.org/10.1021/acs.nanolett.3c03509.

[2] T. Ramasamy, H.B. Ruttala, S. Munusamy, N. Chakraborty, J.O. Kim, Nano drug delivery systems for antisense oligonucleotides (ASO) therapeutics, J. Control. Release 352 (2022) 861-878. https://doi.org/10.1016/j.jconrel.2022.10.050.

[3] E. Samaridou, J. Heyes, P. Lutwyche, Lipid nanoparticles for nucleic acid delivery: current perspectives, Adv. Drug Deliv. Rev. 154-155 (2020) 37-63. https://doi.org/10.1016/j.addr.2020.06.002.

[4] X. Xu, T. Xia, Recent advances in site-specific lipid nanoparticles for mRNA delivery, ACS Nanosci. Au 3 (2023) 192-203. https://doi.org/10.1021/acsnanoscienceau.2c00062.

[5] A. Hussain, H. Yang, M. Zhang, Q. Liu, G. Alotaibi, M. Irfan, H. He, J. Chang, X.J. Liang, Y. Weng, Y. Huang, mRNA vaccines for COVID-19 and diverse diseases, J. Control. Release 345 (2022) 314-333. https://doi.org/10.1016/j.jconrel.2022.03.032.

[6] L.M. Lewis, A.V. Badkar, D. Cirelli, R. Combs, T.F. Lerch, The race to develop the Pfizer-BioNTech COVID-19 vaccine: from the pharmaceutical scientists' perspective, J. Pharm. Sci. 112 (2023) 640-647. https://doi.org/10.1016/j.xphs.2022.09.014.

[7] H. Muramatsu, K. Lam, C. Bajusz, D. Laczko, K. Kariko, P. Schreiner, A. Martin, P. Lutwyche, J. Heyes, N. Pardi, Lyophilization provides long-term stability for a lipid nanoparticle-formulated, nucleoside-modified mRNA vaccine, Mol. Ther. 30 (2022) 1941-1951. https://doi.org/10.1016/j.ymthe.2022.02.001.

[8] D. Li, C. Liu, Y. Li, R. Tenchov, J.M. Sasso, D. Zhang, D. Li, L. Zou, X. Wang, Q. Zhou, Messenger RNA-based therapeutics and vaccines: What's beyond COVID-19?,

ACS Pharmacol. Transl. Sci. 6 (2023) 943-969. https://doi.org/10.1021/acsptsci.3c00047.

[9] G.T. Szabo, A.J. Mahiny, I. Vlatkovic, COVID-19 mRNA vaccines: platforms and current developments, Mol. Ther. 30 (2022) 1850-1868. https://doi.org/10.1016/j.ymthe.2022.02.016.

[10] X. Xu, X. Wang, Y.P. Liao, L. Luo, T. Xia, A.E. Nel, Use of a liver-targeting immune-tolerogenic mRNA lipid nanoparticle platform to treat peanut-induced anaphylaxis by single- and multiple-epitope nucleotide sequence delivery, ACS Nano 17 (2023) 4942-4957. https://doi.org/10.1021/acsnano.2c12420.

[11] A.J. Pollard, E.M. Bijker, A guide to vaccinology: from basic principles to new developments, Nat. Rev. Immunol. 21 (2021) 83-100. https://doi.org/10.1038/s41577-020-00479-7.

[12] I. Tombacz, D. Laczko, H. Shahnawaz, H. Muramatsu, A. Natesan, A. Yadegari, T.E. Papp, M.G. Alameh, V. Shuvaev, B.L. Mui, Y.K. Tam, V. Muzykantov, N. Pardi, D. Weissman, H. Parhiz, Highly efficient CD4+ T cell targeting and genetic recombination using engineered CD4+ cell-homing mRNA-LNPs, Mol. Ther. 29 (2021) 3293-3304. https://doi.org/10.1016/j.ymthe.2021.06.004.

[13] X. Wang, S. Liu, Y. Sun, X. Yu, S.M. Lee, Q. Cheng, T. Wei, J. Gong, J. Robinson, D. Zhang, X. Lian, P. Basak, D.J. Siegwart, Preparation of selective organ-targeting (SORT) lipid nanoparticles (LNPs) using multiple technical methods for tissue-specific mRNA delivery, Nat. Protoc. 18 (2023) 265-291. https://doi.org/10.1038/s41596-022-00755-x.

[14] M. Ongun, A.G. Lokras, S. Baghel, Z. Shi, S.T. Schmidt, H. Franzyk, T. Rades, F. Sebastiani, A. Thakur, C. Foged, Lipid nanoparticles for local delivery of mRNA to

the respiratory tract: effect of PEG-lipid content and administration route, Eur. J. Pharm. Biopharm. 198 (2024) 114266. https://doi.org/10.1016/j.ejpb.2024.114266.

[15] M. Jeong, Y. Lee, J. Park, H. Jung, H. Lee, Lipid nanoparticles (LNPs) for in vivo RNA delivery and their breakthrough technology for future applications, Adv. Drug Deliv. Rev. 200 (2023) 114990. https://doi.org/10.1016/j.addr.2023.114990.

[16] R.L. Goldman, N.T. Vittala Murthy, T.P. Northen, A. Balakrishnan, S. Chivukula, H. Danz, T. Tibbitts, A. Dias, J. Vargas, D. Cooper, H. Gopani, A. Beaulieu, K.V. Kalnin, T. Plitnik, S. Karmakar, R. Dasari, R. Landis, S. Karve, F. DeRosa, Understanding structure activity relationships of good HEPES lipids for lipid nanoparticle mRNA vaccine applications, Biomaterials 301 (2023) 122243. https://doi.org/10.1016/j.biomaterials.2023.122243.

[17] S. Soroudi, M.R. Jaafari, L. Arabi, Lipid nanoparticle (LNP) mediated mRNA delivery in cardiovascular diseases: advances in genome editing and CAR T cell therapy, J. Control. Release 372 (2024) 113-140. https://doi.org/10.1016/j.jconrel.2024.06.023.

[18] C. Guo, H. Yuan, Y. Wang, Y. Feng, Y. Zhang, T. Yin, H. He, J. Gou, X. Tang, The interplay between PEGylated nanoparticles and blood immune system, Adv. Drug Deliv. Rev. 200 (2023) 115044. https://doi.org/10.1016/j.addr.2023.115044.

[19] T. Suzuki, Y. Suzuki, T. Hihara, K. Kubara, K. Kondo, K. Hyodo, K. Yamazaki, T. Ishida, H. Ishihara, PEG shedding-rate-dependent blood clearance of PEGylated lipid nanoparticles in mice: faster PEG shedding attenuates anti-PEG IgM production, Int. J. Pharm. 588 (2020) 119792. https://doi.org/10.1016/j.ijpharm.2020.119792.

[20] Y. Fang, J. Xue, S. Gao, A. Lu, D. Yang, H. Jiang, Y. He, K. Shi, Cleavable PEGylation: a strategy for overcoming the "PEG dilemma" in efficient drug delivery, Drug Deliv. 24 (2017) 22-32. https://doi.org/10.1080/10717544.2017.1388451.

[21] R. Tenchov, J.M. Sasso, Q.A. Zhou, PEGylated lipid nanoparticle formulations: immunological safety and efficiency perspective, Bioconjug. Chem. 34 (2023) 941-960. https://doi.org/10.1021/acs.bioconjchem.3c00174.

[22] R.C. Ryals, S. Patel, C. Acosta, M. McKinney, M.E. Pennesi, G. Sahay, The effects of PEGylation on LNP based mRNA delivery to the eye, PLoS One 15 (2020) e0241006. https://doi.org/10.1371/journal.pone.0241006.

[23] M. Berger, M. Degey, J. Leblond Chain, E. Maquoi, B. Evrard, A. Lechanteur, G. Piel, Effect of PEG anchor and serum on lipid nanoparticles: development of a nanoparticles tracking method, Pharmaceutics 15 (2023) 597. https://doi.org/10.3390/pharmaceutics15020597.

[24] R. Tenchov, R. Bird, A.E. Curtze, Q. Zhou, Lipid nanoparticles-from liposomes to mRNA vaccine delivery, a landscape of research diversity and advancement, ACS Nano 15 (2021) 16982-17015. https://doi.org/10.1021/acsnano.1c04996.

[25] R. Sang, B. Stratton, A. Engel, W. Deng, Liposome technologies towards colorectal cancer therapeutics, Acta Biomater. 127 (2021) 24-40. https://doi.org/10.1016/j.actbio.2021.03.055.

[26] L.E. Waggoner, K.F. Miyasaki, E.J. Kwon, Analysis of PEG-lipid anchor length on lipid nanoparticle pharmacokinetics and activity in a mouse model of traumatic brain injury, Biomater. Sci. 11 (2023) 4238-4253. https://doi.org/10.1039/d2bm01846b.

[27] A. Sarode, Y. Fan, A.E. Byrnes, M. Hammel, G.L. Hura, Y. Fu, P. Kou, C. Hu, F.I. Hinz, J. Roberts, S.G. Koenig, K. Nagapudi, C.C. Hoogenraad, T. Chen, D. Leung, C.W. Yen, Predictive high-throughput screening of PEGylated lipids in oligonucleotide-loaded lipid nanoparticles for neuronal gene silencing, Nanoscale Adv. 4 (2022) 2107-2123. https://doi.org/10.1039/d1na00712b.

[28] L. Geng, N. Kato, Y. Kodama, H. Mukai, S. Kawakami, Influence of lipid composition of messenger RNA-loaded lipid nanoparticles on the protein expression via intratracheal administration in mice, Int. J. Pharm. 637 (2023) 122896. https://doi.org/10.1016/j.ijpharm.2023.122896.

[29] S.A. Dilliard, Q. Cheng, D.J. Siegwart, On the mechanism of tissue-specific mRNA delivery by selective organ targeting nanoparticles, Proc. Natl. Acad. Sci. U. S. A. 118 (2021) e2109256118. https://doi.org/10.1073/pnas.2109256118.

[30] S.A. Dilliard, Y. Sun, M.O. Brown, Y.C. Sung, S. Chatterjee, L. Farbiak, A. Vaidya, X. Lian, X. Wang, A. Lemoff, D.J. Siegwart, The interplay of quaternary ammonium lipid structure and protein corona on lung-specific mRNA delivery by selective organ targeting (SORT) nanoparticles, J. Control. Release 361 (2023) 361-372. https://doi.org/10.1016/j.jconrel.2023.07.058.

[31] S. Liu, R.J. Ono, H. Wu, J.Y. Teo, Z.C. Liang, K. Xu, M. Zhang, G. Zhong, J.P. Tan, M. Ng, C. Yang, J. Chan, Z. Ji, C. Bao, K. Kumar, S. Gao, A. Lee, M. Fevre, H. Dong, J.Y. Ying, L. Li, W. Fan, J.L. Hedrick, Y.Y. Yang, Highly potent antimicrobial polyionenes with rapid killing kinetics, skin biocompatibility and in vivo bactericidal activity, Biomaterials 127 (2017) 36-48. https://doi.org/10.1016/j.biomaterials.2017.02.027.

[32] Y. Ju, W.S. Lee, E.H. Pilkington, H.G. Kelly, S. Li, K.J. Selva, K.M. Wragg, K. Subbarao, T.H.O. Nguyen, L.C. Rowntree, L.F. Allen, K. Bond, D.A. Williamson, N.P. Truong, M. Plebanski, K. Kedzierska, S. Mahanty, A.W. Chung, F. Caruso, A.K. Wheatley, J.A. Juno, S.J. Kent, Anti-PEG antibodies boosted in humans by SARS-CoV-2 lipid nanoparticle mRNA vaccine, ACS Nano 16 (2022) 11769-11780. https://doi.org/10.1021/acsnano.2c04543.

[33] M. Maeki, S. Uno, A. Niwa, Y. Okada, M. Tokeshi, Microfluidic technologies and devices for lipid nanoparticle-based RNA delivery, J. Control. Release 344 (2022) 80-96. https://doi.org/10.1016/j.jconrel.2022.02.017.

[34] L. Miao, J. Lin, Y. Huang, L. Li, D. Delcassian, Y. Ge, Y. Shi, D.G. Anderson, Synergistic lipid compositions for albumin receptor mediated delivery of mRNA to the liver, Nat. Commun. 11 (2020) 2424. https://doi.org/10.1038/s41467-020-16248-y.

[35] C.M. McCrudden, L. Bennie, P. Chambers, J. Wilson, M. Kerr, M. Ziminska, H. Douglas, S. Kuhn, E. Carroll, G. O'Brien, N. Buckley, N.J. Dunne, H.O. McCarthy, Peptide delivery of a multivalent mRNA SARS-CoV-2 vaccine, J. Control. Release 362 (2023) 536-547. https://doi.org/10.1016/j.jconrel.2023.08.053.

[36] D. Pozzi, V. Colapicchioni, G. Caracciolo, S. Piovesana, A.L. Capriotti, S. Palchetti, S. De Grossi, A. Riccioli, H. Amenitsch, A. Lagana, Effect of polyethyleneglycol (PEG) chain length on the bio-nano-interactions between PEGylated lipid nanoparticles and biological fluids: From nanostructure to uptake in cancer cells, Nanoscale 6 (2014) 2782-2792. https://doi.org/10.1039/c3nr05559k.

[37] K.J. Hassett, J. Higgins, A. Woods, B. Levy, Y. Xia, C.J. Hsiao, E. Acosta, O. Almarsson, M.J. Moore, L.A. Brito, Impact of lipid nanoparticle size on mRNA vaccine immunogenicity, J. Control. Release 335 (2021) 237-246. https://doi.org/10.1016/j.jconrel.2021.05.021.

[38] S.J. Shepherd, C.C. Warzecha, S. Yadavali, R. El-Mayta, M.G. Alameh, L. Wang, D. Weissman, J.M. Wilson, D. Issadore, M.J. Mitchell, Scalable mRNA and siRNA lipid nanoparticle production using a parallelized microfluidic device, Nano Lett. 21 (2021) 5671-5680. https://doi.org/10.1021/acs.nanolett.1c01353.

[39] S. Patel, N. Ashwanikumar, E. Robinson, Y. Xia, C. Mihai, J.P. Griffith, 3rd, S. Hou, A.A. Esposito, T. Ketova, K. Welsher, J.L. Joyal, O. Almarsson, G. Sahay, Naturally-occurring cholesterol analogues in lipid nanoparticles induce polymorphic shape and enhance intracellular delivery of mRNA, Nat. Commun. 11 (2020) 983. https://doi.org/10.1038/s41467-020-14527-2.

[40] C. Hald Albertsen, J.A. Kulkarni, D. Witzigmann, M. Lind, K. Petersson, J.B. Simonsen, The role of lipid components in lipid nanoparticles for vaccines and gene therapy, Adv. Drug Deliv. Rev. 188 (2022) 114416. https://doi.org/10.1016/j.addr.2022.114416.

[41] J. Kim, A. Jozic, Y. Lin, Y. Eygeris, E. Bloom, X. Tan, C. Acosta, K.D. MacDonald, K.D. Welsher, G. Sahay, Engineering lipid nanoparticles for enhanced intracellular delivery of mRNA through inhalation, ACS Nano 16 (2022) 14792-14806. https://doi.org/10.1021/acsnano.2c05647.

[42] K. Mrksich, M.S. Padilla, R.A. Joseph, E.L. Han, D. Kim, R. Palanki, J. Xu, M.J. Mitchell, Influence of ionizable lipid tail length on lipid nanoparticle delivery of mRNA of varying length, J. Biomed. Mater. Res. A 112 (2024) 1494-1505. https://doi.org/10.1002/jbm.a.37705.

[43] M. Estape Senti, L. Garcia Del Valle, R.M. Schiffelers, mRNA delivery systems for cancer immunotherapy: lipid nanoparticles and beyond, Adv. Drug Deliv. Rev. 206 (2024) 115190. https://doi.org/10.1016/j.addr.2024.115190.

[44] E. Kon, U. Elia, D. Peer, Principles for designing an optimal mRNA lipid nanoparticle vaccine, Curr. Opin. Biotechnol. 73 (2022) 329-336. https://doi.org/10.1016/j.copbio.2021.09.016.

[45] G. Tilstra, J. Couture-Senecal, Y.M.A. Lau, A.M. Manning, D.S.M. Wong, W.W. Janaeska, T.A. Wuraola, J. Pang, O.F. Khan, Iterative design of ionizable lipids for

intramuscular mRNA delivery, J. Am. Chem. Soc. 145 (2023) 2294-2304. https://doi.org/10.1021/jacs.2c10670.

[46] D.J. Irvine, A. Aung, M. Silva, Controlling timing and location in vaccines, Adv. Drug Deliv. Rev. 158 (2020) 91-115. https://doi.org/10.1016/j.addr.2020.06.019.

[47] E.H. Pilkington, E.J.A. Suys, N.L. Trevaskis, A.K. Wheatley, D. Zukancic, A. Algarni, H. Al-Wassiti, T.P. Davis, C.W. Pouton, S.J. Kent, N.P. Truong, From influenza to COVID-19: lipid nanoparticle mRNA vaccines at the frontiers of infectious diseases, Acta Biomater. 131 (2021) 16-40. https://doi.org/10.1016/j.actbio.2021.06.023.

[48] T. Nakamura, H. Harashima, Dawn of lipid nanoparticles in lymph node targeting: potential in cancer immunotherapy, Adv. Drug Deliv. Rev. 167 (2020) 78-88. https://doi.org/10.1016/j.addr.2020.06.003.

[49] Y. Lee, M. Jeong, J. Park, H. Jung, H. Lee, Immunogenicity of lipid nanoparticles and its impact on the efficacy of mRNA vaccines and therapeutics, Exp. Mol. Med. 55 (2023) 2085-2096. https://doi.org/10.1038/s12276-023-01086-x.

[50] N. Pardi, S. Tuyishime, H. Muramatsu, K. Kariko, B.L. Mui, Y.K. Tam, T.D. Madden, M.J. Hope, D. Weissman, Expression kinetics of nucleoside-modified mRNA delivered in lipid nanoparticles to mice by various routes, J. Control. Release 217 (2015) 345-351. https://doi.org/10.1016/j.jconrel.2015.08.007.

[51] B.L. Mui, Y.K. Tam, M. Jayaraman, S.M. Ansell, X. Du, Y.Y. Tam, P.J. Lin, S. Chen, J.K. Narayanannair, K.G. Rajeev, M. Manoharan, A. Akinc, M.A. Maier, P. Cullis, T.D. Madden, M.J. Hope, Influence of polyethylene glycol lipid desorption rates on pharmacokinetics and pharmacodynamics of siRNA lipid nanoparticles, Mol Ther Nucleic Acids 2 (2013) e139. https://doi.org/10.1038/mtna.2013.66.

[52] X. Zhu, W. Tao, D. Liu, J. Wu, Z. Guo, X. Ji, Z. Bharwani, L. Zhao, X. Zhao, O.C. Farokhzad, J. Shi, Surface de-PEGylation controls nanoparticle-mediated siRNA delivery in vitro and in vivo, Theranostics 7 (2017) 1990-2002. https://doi.org/10.7150/thno.18136.

[53] M.S. Webb, D. Saxon, F.M. Wong, H.J. Lim, Z. Wang, M.B. Bally, L.S. Choi, P.R. Cullis, L.D. Mayer, Comparison of different hydrophobic anchors conjugated to poly(ethylene glycol): effects on the pharmacokinetics of liposomal vincristine, Biochim. Biophys. Acta 1372 (1998) 272-282. https://doi.org/10.1016/s0005-2736(98)00077-7.

[54] A. Akinc, M. Goldberg, J. Qin, J.R. Dorkin, C. Gamba-Vitalo, M. Maier, K.N. Jayaprakash, M. Jayaraman, K.G. Rajeev, M. Manoharan, V. Koteliansky, I. Rohl, E.S. Leshchiner, R. Langer, D.G. Anderson, Development of lipidoid-siRNA formulations for systemic delivery to the liver, Mol. Ther. 17 (2009) 872-879. https://doi.org/10.1038/mt.2009.36.

[55] K. Lv, Z. Yu, J. Wang, N. Li, A. Wang, T. Xue, Q. Wang, Y. Shi, L. Han, W. Qin, J. Gong, H. Song, T. Zhang, C. Chang, H. Chen, X. Zhong, J. Ding, R. Chen, M. Liu, W. Zhang, S. Cen, Y. Dong, Discovery of ketal-ester ionizable lipid nanoparticle with reduced hepatotoxicity, enhanced spleen tropism for mRNA vaccine delivery, Adv Sci (Weinh) 11 (2024) e2404684. https://doi.org/10.1002/advs.202404684.

[56] G. Miao, Y. He, K. Lai, Y. Zhao, P. He, G. Tan, X. Wang, Accelerated blood clearance of PEGylated nanoparticles induced by PEG-based pharmaceutical excipients, J. Control. Release 363 (2023) 12-26. https://doi.org/10.1016/j.jconrel.2023.09.003.

[57] S.A. Gaballa, T. Shimizu, H. Ando, H. Takata, S.E. Emam, E. Ramadan, Y.W. Naguib, F.M. Mady, K.A. Khaled, T. Ishida, Treatment-induced and pre-existing anti-

peg antibodies: prevalence, clinical implications, and future perspectives, J. Pharm. Sci. 113 (2024) 555-578. https://doi.org/10.1016/j.xphs.2023.11.001.

[58] H. Takata, T. Shimizu, R. Yamade, N.E. Elsadek, S.E. Emam, H. Ando, Y. Ishima, T. Ishida, Anti-PEG IgM production induced by PEGylated liposomes as a function of administration route, J. Control. Release 360 (2023) 285-292. https://doi.org/10.1016/j.jconrel.2023.06.027.

[59] H. Wang, Y. Wang, C. Yuan, X. Xu, W. Zhou, Y. Huang, H. Lu, Y. Zheng, G. Luo, J. Shang, M. Sui, Polyethylene glycol (PEG)-associated immune responses triggered by clinically relevant lipid nanoparticles in rats, NPJ Vaccines 8 (2023) 169. https://doi.org/10.1038/s41541-023-00766-z.

Supplementary material

Role of PEGylated lipid in lipid nanoparticle formulation for *in vitro* and *in vivo* delivery of mRNA vaccines

Li Zhang [a], Brandon Yi Loong Seow [a], Ki Hyun Bae [a], Yue Zhang [a], Kuo-Chieh Liao [b], Yue Wan [b], Yi Yan Yang [a, *]

[a] Bioprocessing Technology Institute (BTI), Agency for Science, Technology and Research (A*STAR), 20 Biopolis Way, #06-01 Centros, Singapore 138668, Republic of Singapore

[b] Genome Institute of Singapore (GIS), Agency for Science, Technology and Research (A*STAR), 60 Biopolis Street, #02-01 Genome, Singapore 138672, Republic of Singapore

Corresponding author at:

Bioprocessing Technology Institute (BTI), Agency for Science, Technology and Research (A*STAR), 20 Biopolis Way, #06-01 Centros, Singapore 138668, Republic of Singapore

* Email address: yyyang@bti.a-star.edu.sg (**Yi Yan Yang**)

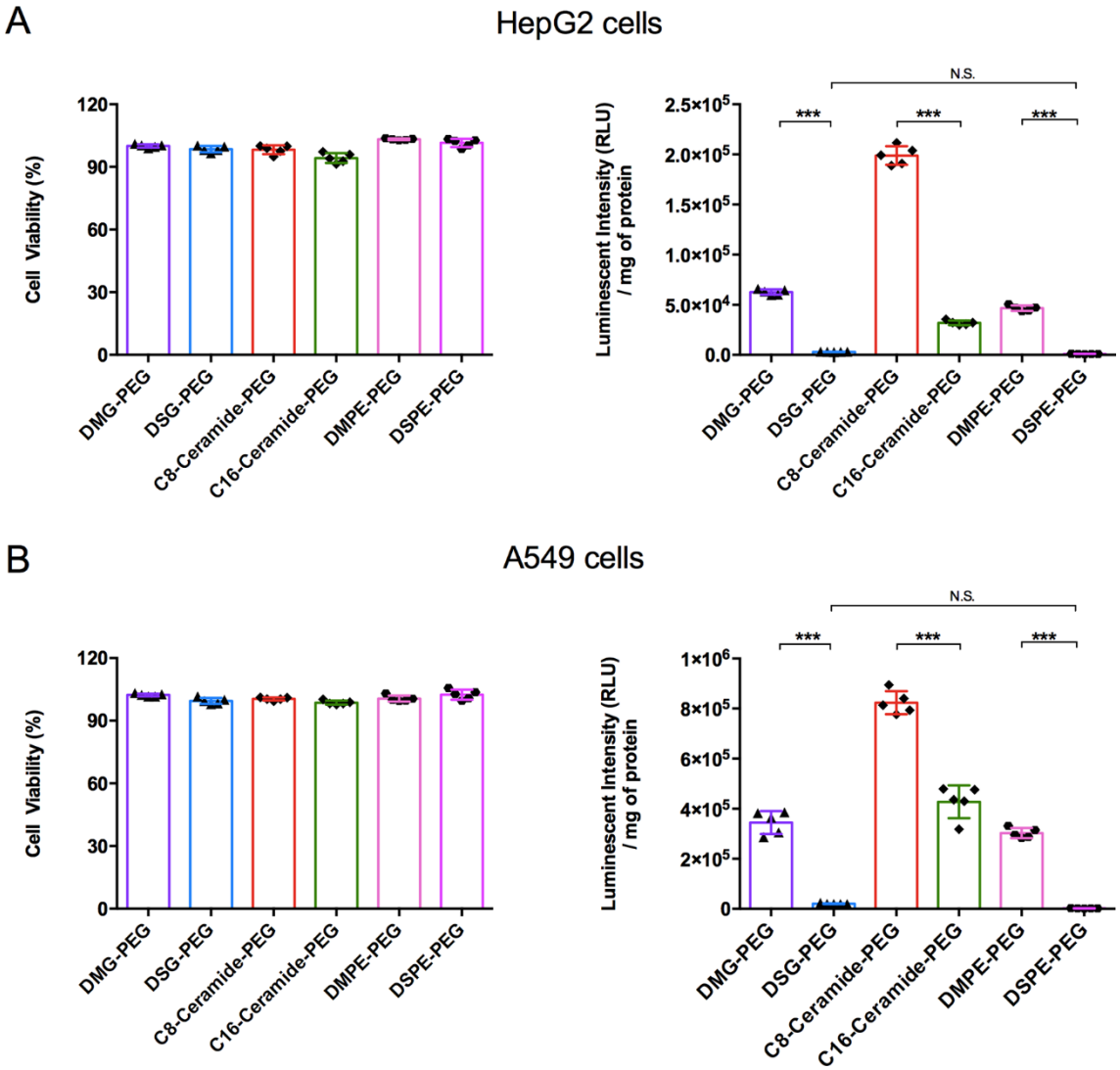

Figure S1. Effect of lipid tail length of PEG-lipid on cytocompatibility and normalized translation efficiency of FLuc mRNA-LNPs prepared with different PEG-lipids at 1.6% molar content via manual mixing in HepG2 (A) and A549 (B) cells. (n = 5 per group).

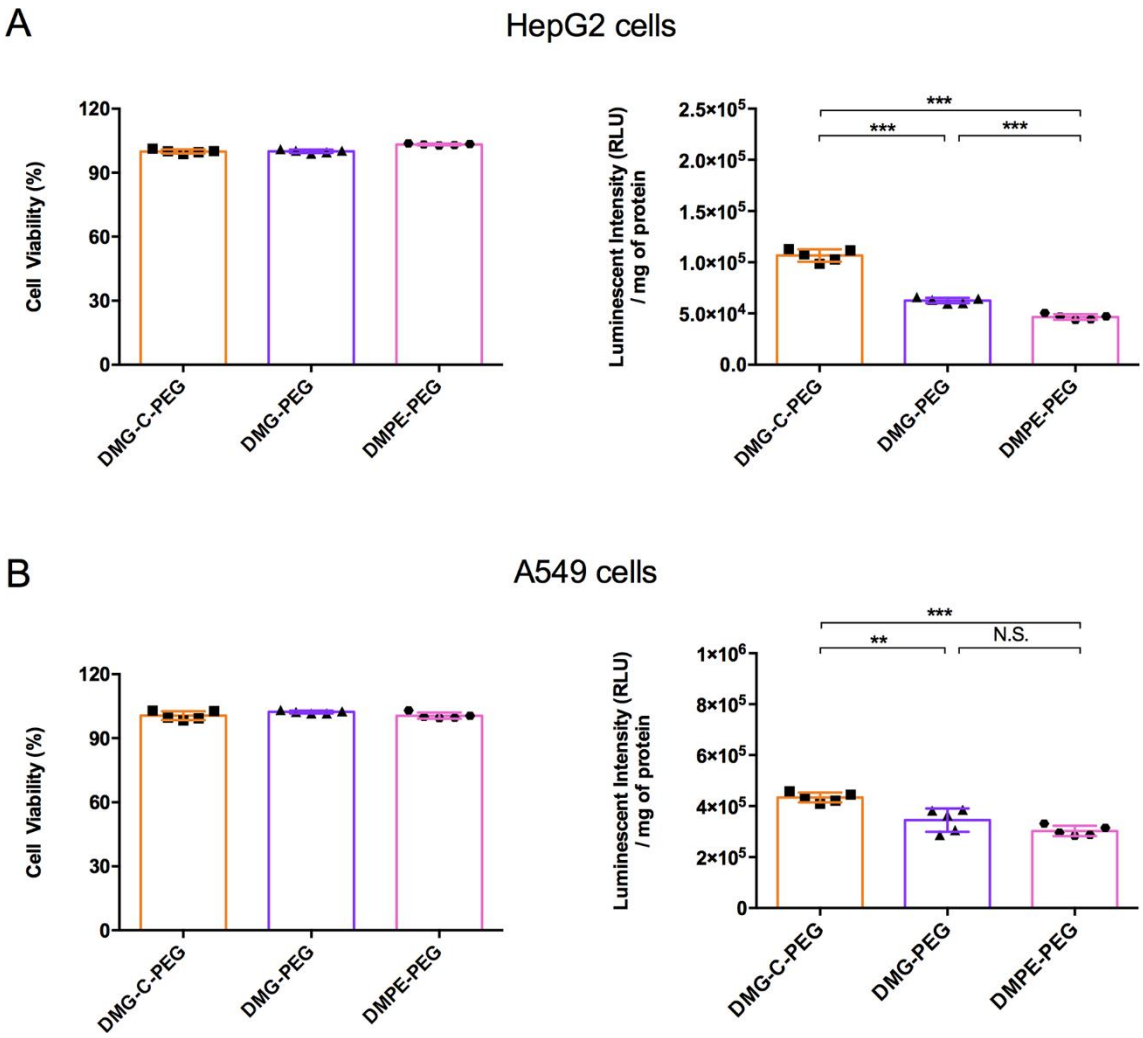

Figure S2. Effect of the chemical linker between PEG and lipid tails in PEG-lipid on cytocompatibility and normalized translation efficiency of FLuc mRNA-LNPs prepared with different PEG-lipids at 1.6% molar content *via* manual mixing in HepG2 (A) and A549 (B) cells. (n = 5 per group).

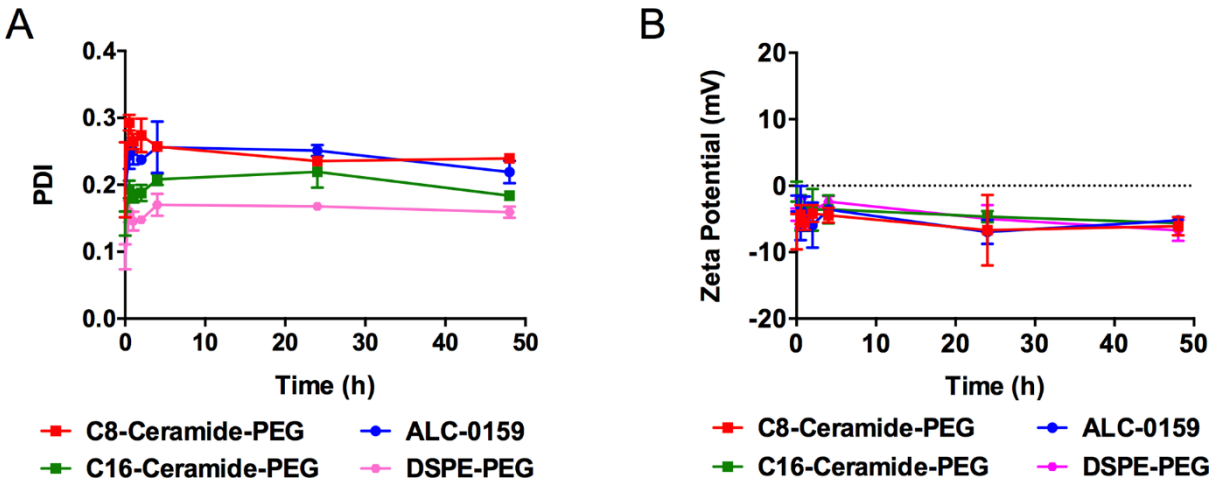

Figure S3. PDI (A) and zeta potential (B) changes of mRNA-LNPs incubated in PBS containing 10% FBS at 37 °C within 48 h. (n = 3 per group).

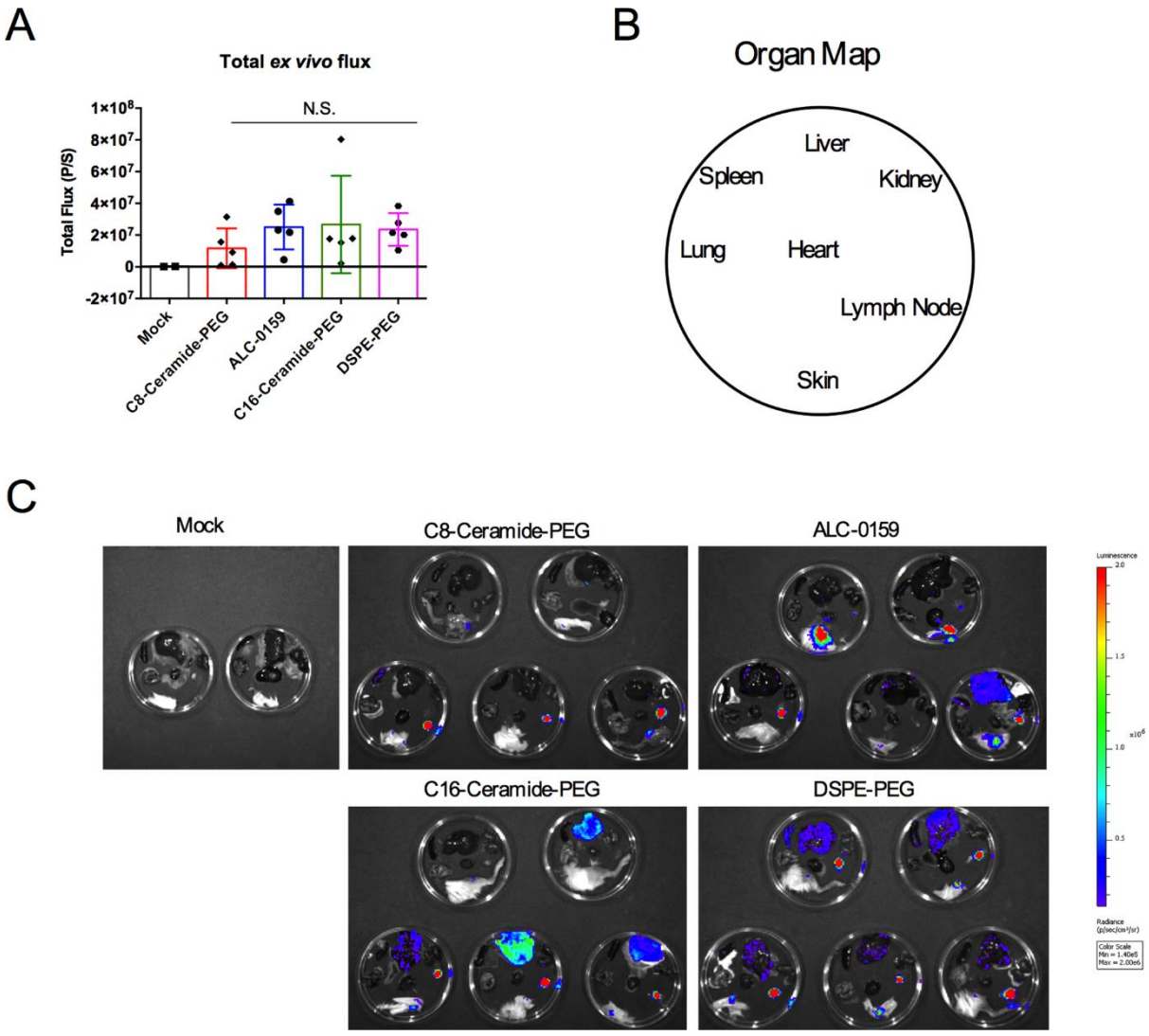

Figure S4. *Ex vivo* translated luciferase of mRNA-LNPs formulated *via* microfluidic mixing after subcutaneous administration. (A) *Ex vivo* total flux of collected organs at 24 h quantified by bioluminescence imaging. (B) *Ex vivo* organ bioluminescence imaging map of Balb/c mice injected with different Fluc mRNA-LNPs. (C) *Ex vivo* bioluminescence images of Balb/c mice injected with different Fluc mRNA-LNPs at 24 h post administration. (n = 2-5 per group).

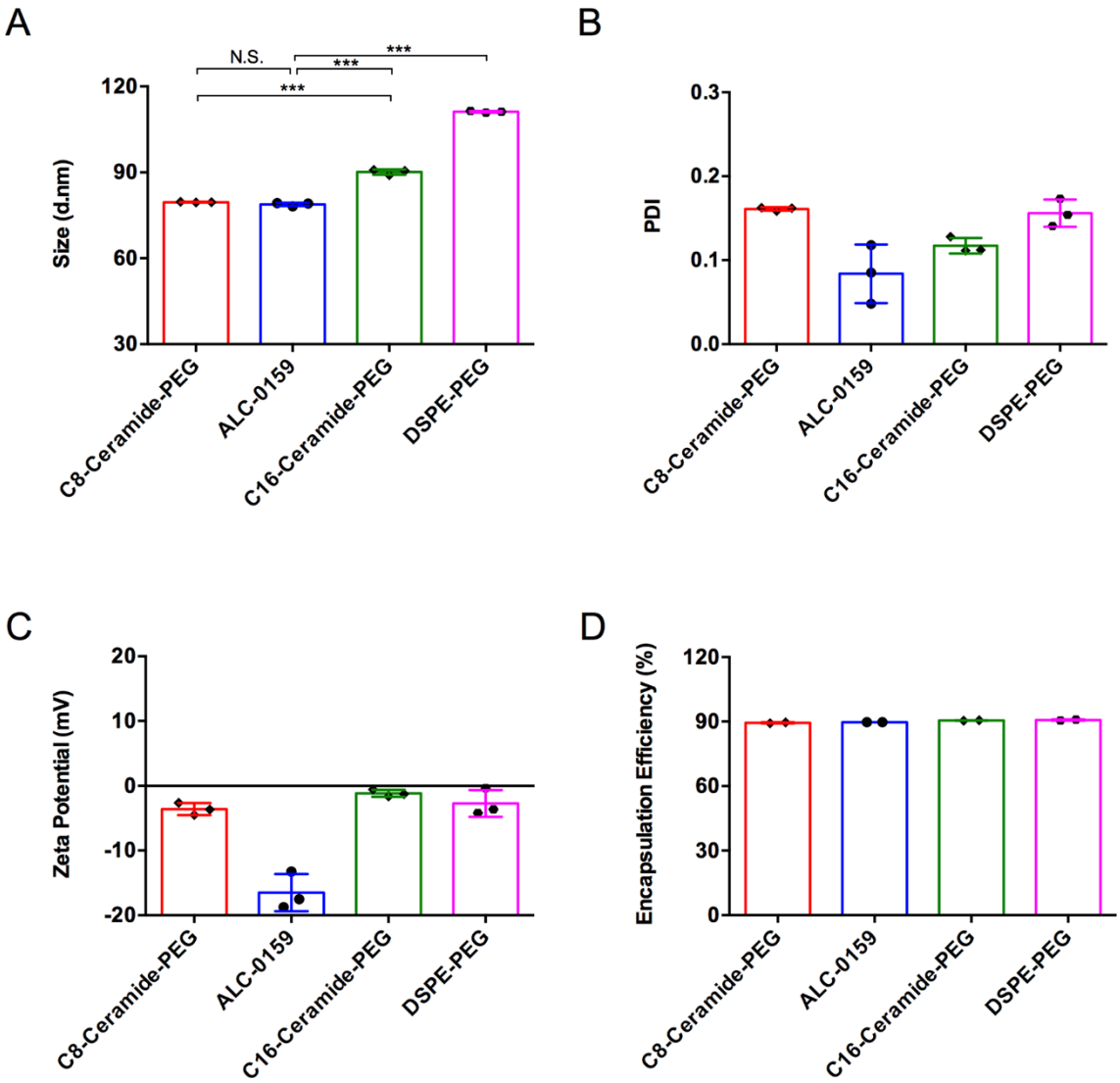

Figure S5. Physicochemical properties of LNPs loaded with mRNA encoding spike protein of SARS-CoV-2 Delta variant prepared with different PEG-lipids at 1.6% molar content via microfluidic mixing, including size (A), PDI (B), zeta potential (C), and encapsulation efficiency (D). (n = 2-3 per group).